PEOPLE'S DEMOCRATIC REPUBLIC OF ALGERIA

Ministry of Higher Education and Scientific Research

IBN KHALDOUN UNIVERSITY OF TIARET

FACULTÉ DES SCIENCES APPLIQUÉES

Electrical Engineering Department

Thesis

Presented for obtaining the diploma of

Master

Spécialité : **Electrotechnique**

Theme

Off-Grid Green Hydrogen Production in the Algerian Sahara using a Hybrid Photovoltaic-Wind System with DC-DC Conversion for Sustainable Energy Solutions

Presented by :

Mr. Abdelazziz Rafik GHEZLI

Mlle. Bouchra BOUSTA

Supported on **23/06/2025** before the jury composed of :

First and last name	Grade	Establishment	Quality
Mr. Abderrahmane BERKANI	MCA	Univ. of Tiaret	President
Mr. Karim NEGADI	Pr	Univ. of Tiaret	Supervisor
Mr. Rabah ARARIA	MCB	Univ. of Tiaret	Co-Supervisor
Mr. Mohamed KOUADRIA	MCA	Univ. of Tiaret	Examiner
Mr. Mohamed BEY	MCA	Univ. of Tiaret	Examiner

Academic Year 2024/2025

Acknowledgements

First and foremost, we express our deep gratitude to **Allah**, the Almighty and Most Merciful, who has bestowed upon us countless blessings by granting us health, patience, inner peace, as well as the strength and perseverance necessary to complete this work.

We would like to extend our sincere thanks to Professor **Karim NEGADI**, of Ibn Khaldoun University of Tiaret, and to Mr. **Rabah ARARIA**, Senior Lecturer (Class B) at the same university, for having accepted to supervise and guide our thesis. Their insightful guidance, constant availability, and kind support have been of great value throughout this academic journey.

We are also deeply grateful to Mr. **Abderrahmane BERKANI**, Senior Lecturer (Class A) at Ibn Khaldoun University of Tiaret, for the honor he has done us by agreeing to chair the jury for this defense.

Our heartfelt thanks go to Mr. **Mohamed KOUADRIA**, Senior Lecturer (Class A) at Ibn Khaldoun University of Tiaret, for the attention he has given to our work by accepting to serve as an examiner.

We warmly thank Mr. **Mohamed BEY**, Senior Lecturer (Class A) at Ibn Khaldoun University of Tiaret, for his participation in the evaluation of this thesis and for the scientific enrichment he brings through his presence on the jury.

Our gratitude also goes to all the faculty members of the **Department of Electrical Engineering**, whose dedication and professionalism have greatly contributed to our academic development. Their constant encouragement has been a key factor in our success.

Finally, we would like to thank all those—whether known or working behind the scenes—who, in one way or another, contributed to the realization and success of this project. To each and every one of you, we extend our most sincere thanks.

Table of Contents

Acknowledgements i

Table des figures v

Liste des tableaux vi

General introduction 2

1 General introduction . . . 2

I Renewable energy resources in the Algerian Sahara 4

1 Introduction . . . 5

2 Overview of solar and wind energy potential in the region : . . . 5

2.1 Solar : . . . 6

2.2 Wind . . . 7

2.3 Water source : . . . 8

2.4 Green hydrogen : . . . 9

2.4.1 Applications for Green Hydrogen : . . . 10

2.4.2 Types of Hydrogen . . . 10

2.4.3 transport of hydrogen : . . . 11

3 Climatic and environmental factors affecting producing green hydrogen . . . 11

3.1 Panel degradation : . . . 11

3.1.1 Dust characteristics, accumulation, and impact on PV module . . . 11

3.1.2 Influencing factors and consequences . . . 13

3.1.3 Ecological influences : noise impact . . . 14

3.1.4 Ecological influences : visual impact . . . 15

3.1.5 Ecological influences : soil erosion and deforestation . . . 16

3.1.6 The dangers and effects of producing hydrogen : . . . 16

4 Case studies and existing renewable energy projects in the Algerian Sahara. . . . 17

4.1 wind Kaberten . . . 19

5 Conclusion . . . 19

II Components modelling electrolyzer and renewable energy profiles 21

1 Introduction . . . 22

2 The principle of water electrolysis : . . . 22

2.1 Electrolysis of Proton Exchange Membrane (PEM) . . . 25

2.1.1 PEM Electrolyser Validation and Modeling . . . 26

2.1.2 Resistive model . . . 29
2.1.3 Dynamic model . . . 29
2.1.4 Electrochemical model . . . 33
3 athematical Model of PV Power Generation : . . . 34
4 DC-DC Boost Converter Modeling . . . 38
4.1 Boost converter . . . 38
5 Model of Wind Turbine Aerodynamics . . . 39
6 Permanent magnet synchronous generator : . . . 40
7 MPPT technique . . . 41
8 Design of DC/AC Inverters . . . 42
9 Conclusion . . . 43

III Simulation results of a PEM electrolyzer powered by direct constant voltage and a hybrid source **45**

1 Introduction . . . 46
2 Simulation of the electrolyzer for hydrogen production . . . 47
3 Simulation results of electrolyzer powered by a constant voltage source . . . 47
4 Integration of a hybrid renewable energy conversion chain. . . . 52
5 Simulation results of electrolyzer integration . . . 53
6 Voltage, Current, and Power Profiles . . . 53
6.1 Hydrogen Flow Rate, Pressure, and Storage Dynamics . . . 55
6.2 Grid Characteristics . . . 56
6.3 Energy management in hybrid PV/wind electrolysis systems . . . 59
7 Conclusions . . . 61

General conclusion **64**

Bibliographie **68**

List of Figures

Figure. I.1 : Global cumulative renewable power installed capacity growth (GW) [1]. 6
Figure. I.2 : The temperature distribution in Algeria [2]. 7
Figure. I.3 : Annual average of wind speed at 10 m above ground level in Algeria [3]. 8
Figure. I.4 : summary of Hydrogen colors and their production route (source : (Droege, 2021)[4] 10
Figure. I.5 : Dust accumulation on PV panels [9]. 13
Figure. I.6 : Schematic representation of wind energy development and potential impacts, that is, (1) noise and visual, (2) bird fatality, (3) soil erosion and defor- estation, (4) lightening from towers, (5) electromagnetic, and (6) surrounding neighborhood. 16
Figure. I.7 : Locations of PV stations in Algeria. 18
Figure. I.8 : Panoramic photograph of the 10 MW wind turbine farm (Kaberten) [5]. 19

Figure. II.1 : The schematic procedure for Green Hydrogen production [6]. 24
Figure. II.2 : Classification and comparison of electrolyzer gypes for hydrogen production. 25
Figure. II.3 : Schematic diagram of PEM water electrolysis and the fundamental thermodynamic properties [7]. 26
Figure. II.4 : Resistive equivalent circuit for a PEMEC. 29
Figure. II.5 : Dynamic equivalent circuit for a PEMEC. 29
Figure. II.6 : Dynamic equivalent circuit for a PEMEC [8]. 30
Figure. II.7 : Electrochemical model without the activation overpotential of the cathode and with Randles–Warburg impedance [9]. 30
Figure. II.8 : Dynamic equivalent circuit used for PEMEC accounting for the ohmic + activation + concentration losses as a resistance, divided into anode and cathode contributions [21].. 31
Figure. II.9 : Dynamic equivalent circuit used for PEMEC accounting for the ohmic + activation + concentration losses as a Warburg impedance, divided into anode and cathode contributions[21]. 32
Figure. II.10 :The PV cell's equivalent circuit. 35
Figure. II.11 :Characteristics of the PV cell at different illumination levels : (a) current/voltage characteristic, (a) power/voltage characteristic. 37
Figure. II.12 :Circuit diagram of boost converter[10]. 38
Figure. II.13 :Bloc diagram of wind turbine. 40

Figure. II.14 :Turbine power characteristics. 40
Figure. II.15 :Topology based on synchronous generator with two converters [11]. . . . 40
Figure. II.16 :The diagram of the DC-DCbuckconverter. 41
Figure. II.17 :Curve at various points along with the power characteristic P-V. 42
Figure. II.18 :Flowchart of the P&O technique [12]. 42
Figure. II.19 :DC/AC inverter design. 43

Figure. III.1 : PEMFC and Electrolyzer in MATLAB / Simulink. 48
Figure. III.2 : Buck converter in MATLAB / Simulink. 48
Figure. III.3 : MATLAB/Simulink module for PEM electrolyze. 49
Figure. III.4 : Dynamic response of a PEM electrolyzer system : voltage (a) and current(b) over time. 49
Figure. III.5 : Dynamic response of a PEM electrolyzer system : voltage (a) and current(b) over time. 50
Figure. III.6 : Dynamic response of a PEM electrolyzer system : Hydrogen flow rate (a) , Hydrogen volume (b) over time. 51
Figure. III.7 : Dynamic response of a PEM electrolyzer system hydrogen volume (a), and (d) Pressure (b) over time. 51
Figure. III.8 : Dynamic response of a PEM electrolyzer system : Power over time. . . . 52
Figure. III.9 : Simulink model for the integration of an electrolyzer into an energy system 53
Figure. III.10 :Wind turbine characteristics for hydrogen production – power, torque, and efficiency profiles under varying wind speeds 54
Figure. III.11 :Dynamic response of a PEM electrolyzer system : (a) Current, (b) Hydrogen flow rate, (c) Hydrogen volume, and (d) Pressure over time. . 56
Figure. III.12 :Performance analysis of load : (a) Three-phase stator currents, (b) Three-phase rotor currents and its zoom. 57
Figure. III.13 :Regulated DC bus voltage. 58
Figure. III.14 :Characteristics of the power grid : (a) Voltage, (b) Current grid and its zoom. 58
Figure. III.15 :Power Management flowchart for off-grid Green hydrogen production with a hybrid PV/wind-to-electrolysis system. 60
Figure. III.16 :Power Management overview – wind power, PV power, grid power, load power, and electrolyzer power distribution. 61

List of Tables

Tableau. I.1 : Water Sources and Their Potential for Green Hydrogen Production in Algeria 9
Tableau. I.2 : Performance of PV module in partial shading conditions [13] 12
Tableau. I.3 : List of Solar Power Stations in Algeria (Split View) 18

Tableau. II.1 : Parameter values 36

General introduction

General introduction

1 General introduction

This research delves into the burgeoning field of green hydrogen production, specifically focusing on the innovative application of off-grid systems in the Algerian Sahara. The global drive towards decarbonization and sustainable energy solutions has amplified the significance of green hydrogen, produced through the electrolysis of water using renewable energy. The Algerian Sahara, with its vast and underexploited renewable energy potential, presents a unique opportunity to establish a robust framework for such production. This study aims to explore the technical feasibility and operational benefits of integrating a hybrid photovoltaic-wind system with advanced DC-DC conversion for efficient and sustainable green hydrogen generation in this geographically strategic region. The first chapter lays the groundwork by thoroughly characterizing the renewable energy landscape of the Algerian Sahara. It explores the immense potential of solar insolation and wind speeds that define this region. This section will provide a detailed analysis of the available resources, including irradiance data and wind speed distributions, to quantify their suitability for powering an off-grid hydrogen production facility. Understanding these resources is crucial for the effective design and sizing of the hybrid energy system, ensuring a consistent and ample supply for the electrolysis process.

Building upon the assessment of renewable resources, the second chapter focuses on the intricate modeling of the core components of the green hydrogen production system. This includes developing accurate mathematical models for the Proton Exchange Membrane (PEM) electrolyzer, a key technology for efficient hydrogen production, considering its operational characteristics, energy consumption, and output efficiency. Furthermore, this chapter will detail the modeling of the photovoltaic and wind energy profiles, accounting for their inherent variability and intermittency. The integration of these models is essential for simulating the system's dynamic behavior and predicting its performance under various environmental conditions.

The third chapter presents the crucial simulation results, providing empirical evidence of the system's viability. This section will demonstrate the performance of the PEM electrolyzer under two distinct power scenarios : directly powered by a constant DC voltage and powered by the proposed hybrid photovoltaic-wind system with DC-DC conversion. The simulations will analyze key performance indicators such as hydrogen production rate, system efficiency, and the impact of renewable energy fluctuations on the electrolyzer's operation. This chapter aims to validate the effectiveness of the hybrid system in providing a stable and continuous power supply for green hydrogen production, thereby showcasing its potential for sustainable energy solutions in the Algerian Sahara. .

Chapter I

Renewable energy resources in the Algerian Sahara

1 Introduction

The current chapter provides a comprehensive overview of the potential for green hydrogen production in the Algerian Sahara and identifies three major pillars : solar and wind potential, water availability, and area suitability for hydrogen-based applications. The Algerian Sahara has some of the most elevated solar irradiance rates in the world and favorable wind conditions in some areas, thus an ideal location for the harvesting of renewable energy. In addition to the availability of energy, the chapter examines the crucial factor of water resources—needed for the process of electrolysis—within this dry area, including natural and unconventional sources.

The chapter further explores the potential applications of green hydrogen, namely in the transport sector. With countries seeking to reduce greenhouse gas emissions and transition to low-carbon economies, green hydrogen is introduced as a viable fuel alternative for heavy transport, public transport, and industrial mobility. Climate and environmental factors such as extreme weather, dust, and water scarcity are also explored for their impact on hydrogen production efficiency and sustainability.

Finally, the chapter refers to real case studies and recent renewable energy projects in the Algerian Sahara. The cases provide significant data on current developments, technological feasibility, and the growing strategic role of the region in the global energy shift.

2 Overview of solar and wind energy potential in the region :

People from all walks of life are developing and using clean and renewable energy sources (RES) as a result of the world's population growth, electricity demands, and environmental consciousness. Additionally, renewable resources are available everywhere and to everyone, regardless of political or geographic limits, and they will never run out or create greenhouse gases (GHG). New industries are born, the national economy is strengthened, new employment are created, affordable energy is provided, and reduce the negative consequences of traditional energy sources while doing so. RES use is being promoted for a variety of uses, including providing isolated and tiny applications with high-quality power. through solar air conditioning and desalination, off-grid and grid-connected wind and solar PV farms, hybrid power systems, and power generation utilizing the solar chimney idea. The need for energy storage systems is

growing as a result of new energy industries, RES commercial acceptability, and technological advancements.

Lithium-ion batteries and super-capacitors are now the recommended energy storage devices for hybrid power systems. smart grids, and other uses because of their long lifespan, high energy density, and quick charging and discharging rates. Figure (I.1) makes it clear that the total amount of renewable power is growing steadily. the negative consequences of traditional energy sources. Power generation using the solar chimney concept, offgrid and grid-connected wind and solar PV farms, solitary air disinfection and desalination, and quality power supply to remote and small applications are just a few of the many applications that are encouraging the use of RES.

The need for energy storage systems is growing as a result of new energy industries, RES commercial acceptability, and technological advancements. Because of their high energy density, quick charging and discharging times, and extended lifespan, super-capacitors and lithium-ion batteries have emerged as the go-to energy storage media for smart grids, hybrid power systems, and other applications. Figure (I.1) makes it clear that the total amount of renewable power is growing steadily.

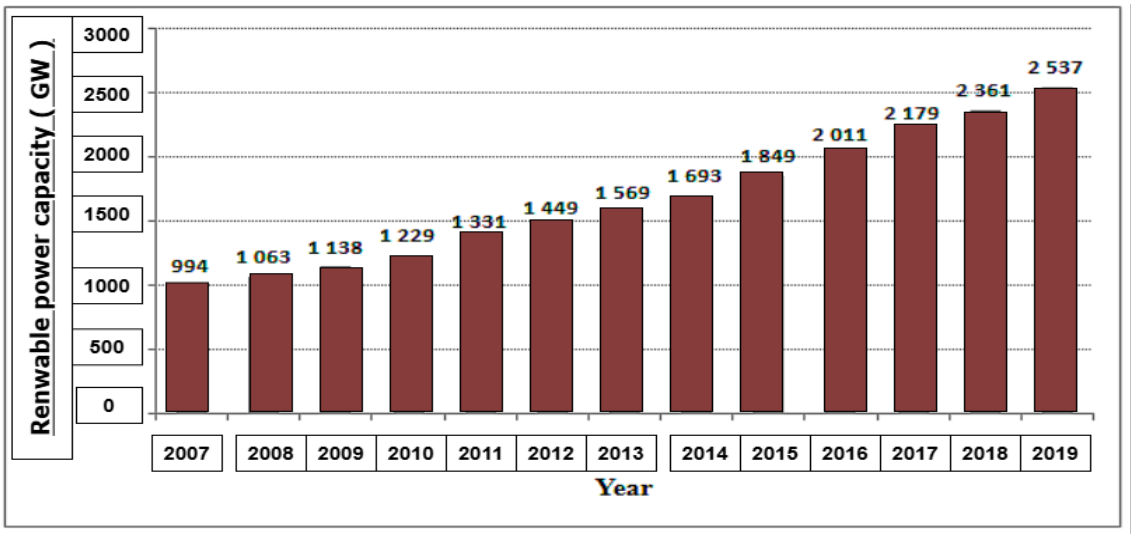

Fig. I.1 *Global cumulative renewable power installed capacity growth (GW) [1].*

2.1 Solar :

The nation's desert is regarded as one of the regions with the highest average temperatures and sun radiation in the world. Insolation lasts between 2000 and 3900 hours a year, and horizontal surface radiation is between 3 and 5 $kWh/m2$. Across the nation, the National

Meteorological Office (ONM) operates a network of 78 meteorological measuring stations. Figure (I.2) displays the distribution of temperature and radiation across the nation.

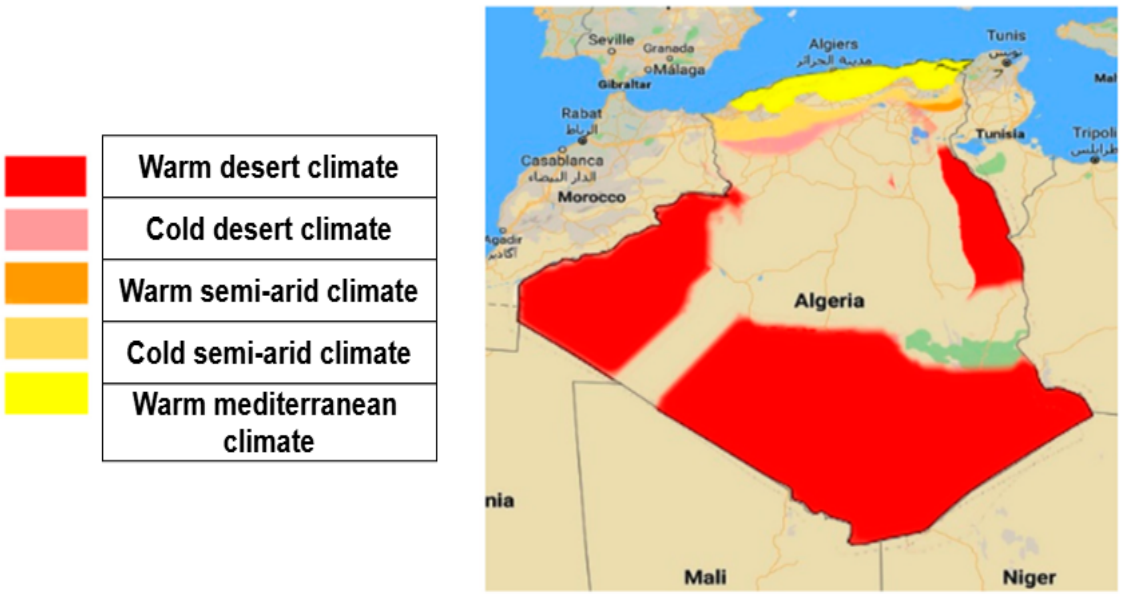

Fig. I.2 *The temperature distribution in Algeria [2].*

2.2 Wind

Understanding the features of the wind regimes in For the purpose of exploiting wind resources, any locations provided by meteorological measurement stations are crucial. Recently, an effort was made in Algeria to enhance the wind map in Boudia et al. created Algeria. Using more modern meteorological data, which were gathered over a ten-year period (2001–2010) at 63 measurement stations spread across Algerian territory and 24 in nearby neighboring countries, these data were acquired at a height of $10m$. It is important to keep in mind that wind speed rises as wind turbine height above ground level does. This implies that all turbines with hub heights greater than 10 m all of which are currently on the market—will experience a notable increase in the yearly mean wind speed. The Algerian Meteorological National Office provides the wind speed readings, which are single-point data at each measuring station. Each site's data was gathered across a variety of time periods, and the results were utilized to assess the average wind speed's annual variations as well as its frequency. The IDW was then used to interpolate wind speeds. One type of geographical interpolation is the Inverse Distance Weighing Method (IDW). It establishes a link between bits of single-point information.

Therefore, the range for the average is indicated by the highest and lowest numbers. It is anticipated that the relationship between two points will weaken as they get farther apart. The

gap between's output is a continuous raster data set that contains values ranging from the study's highest to lowest input wind speeds. The process for determining the IDW in ArcGIS involves selecting the z-value of the recorded wind speeds after receiving the wind speed point data as input. The result The next greatest cell size (DD) was set to 0.072 (Decimal Degree), since the default was set at around 0.056. The default settings for the remaining optional features were maintained . The wind speed estimates used in this investigation were taken from this database at a height of 10 meters. This section's wind map was created using GIS software ;figure (I.3) shows Algeria's annual wind map at a height of 10 meters.

The average yearly wind speed for each region is displayed in figure (I.3). The average wind speed in Algeria ranges from 1.6 m/s to 6.3 m/s, according to the wind speed analysis. The Adrar region recorded the highest wind speeds, which were 6.3 m/s, Hassi-R'mel 6.1 m/s, and Tindouf region 6 m/s. The southwest regions, as well as Tiaret, Borj-Baji Mokhtar, Djelfa, and Biskra, are home to the picturesque windy places. In the coastal line region, the average wind speed is roughly 4 m/s. The northern Tizi-Ouzou region had the slowest speed, at 1.6 m/s. Therefore, we find that the wind potential in the Maghnia region (northwestern region) is less than 1.4 m/s.

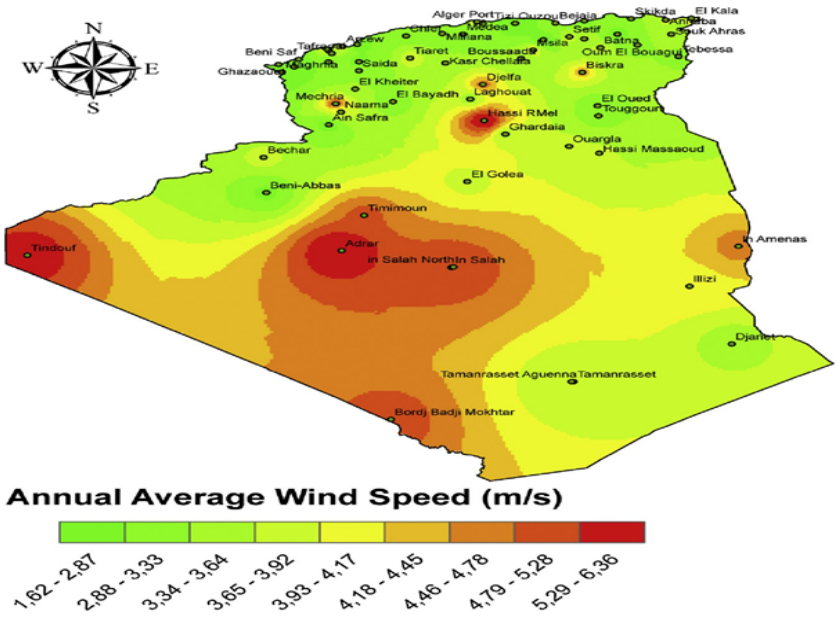

Fig. I.3 *Annual average of wind speed at 10 m above ground level in Algeria [3].*

2.3 Water source :

The following table summarizes the potential water sources in Algeria that can be used for green hydrogen production. This table emphasizes the most viable water sources in Algeria

for green hydrogen production, focusing on the renewable potential of each source and the challenges related to water availability and extraction.

Tableau I.1 – Water Sources and Their Potential for Green Hydrogen Production in Algeria

Water Source	**Type**	**Location**	**Potential for Green Hydrogen**	**Challenges**
North-western Sahara aquifer system (NWSAS)	Groundwater (Fossil)	Algerian Sahara (Ouargla, Adrar, Tamanrasset)	Large reserves can support green hydrogen production in desert regions using solar energy	Limited natural recharge, risk of over-extraction
Complex terminal aquifer	Groundwater (Limestone/Dolomite)	Sahara (Northern & Central regions)	Shallower and more accessible for extraction, ideal for solar-powered hydrogen production in remote areas	High water salinity and extraction costs
Continental intercalaire aquifer	Groundwater (Sandstone)	Southern Algeria (Illizi, Tamanrasset)	Vast, deep aquifer suitable for long-term hydrogen production with limited human impact	Depth and limited recharge make extraction costly and less sustainable
Algerian coastal aquifers	Groundwater (Renewable)	Coastal regions (Oran, Algiers)	Easier access, more sustainable supply, supports localized hydrogen production with wind/solar energy	Competing demands for drinking and irrigation water
Desalinated seawater	Desalinated (Renewable)	Coastal regions (Mediterranean coast)	High potential for hydrogen production, especially in solar-rich areas	High energy cost for desalination ; requires infrastructure development
Surface water (Dams & reservoirs)	Surface Water (Renewable)	Northern Algeria (Chéliff, Keddara)	Suitable for small to medium-scale hydrogen projects where renewable energy is available	Seasonal variability and competition with agriculture and domestic needs

2.4 Green hydrogen :

Green hydrogen, both clean and renewable, is produced using electricity from renewable sources through the electrolysis of water. It can also be generated by converting biogas as a substitute for natural gas, and through biochemical conversion processes of biomass, provided these processes meet sustainability criteria.[14]

2.4.1 Applications for Green Hydrogen :

All areas of the energy industry can make use of hydrogen, which is a flexible energy carrier. At the moment, hydrogen is generally utilized as a feedstock for chemical or refinery product synthesis. But in order to meet decarbonization goals, it will be essential to prioritize and expand applications. of hydrogen for the creation of low-carbon fuels and feedstocks, as well as for direct use, storage, and electricity generation. [15, 14]

2.4.2 Types of Hydrogen

The worldwide demand for Hydrogen is growing. However, not all countries have access to the same technology for Hydrogen production, storage, and transportation, resources, and geopolitical outlook to use it. Consequently, there are limitations and opportunities bound to each method which have been developed to get to Hydrogen for the past century. These matters also affect the final price for the user due to the barriers each section has. All the procedures for Hydrogen generation have been codified based on colors in order to reach a better understanding of each one of them. The colors, describing the main production routes, are as follows : grey (or brown/black), blue hydrogen, green hydrogen, yellow (or purple) hydrogen. Also, the type of Hydrogen produced is sometimes called out by names like Clean Hydrogen, Renewable Hydrogen, and Low-carbon Hydrogen as well [4, 16]. In Figure (I.4), a summary of all types of Hydrogen can be seen in the picture and the detailed explanation follows :

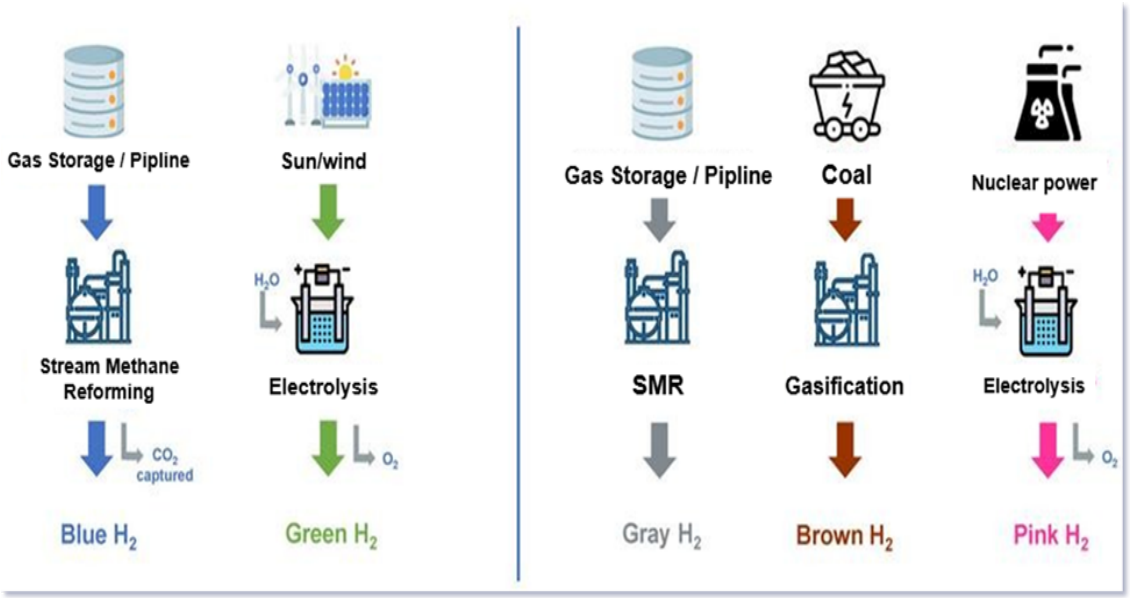

Fig. I.4 *summary of Hydrogen colors and their production route (source : (Droege, 2021)[4]*

2.4.3 transport of hydrogen :

Hydrogen offers a promising solution for storing renewable energy and reducing greenhouse gas emissions, with hydrogen-powered vehicles standing out as a significant application. However, the realization of a hydrogen economy faces a key challenge : the development of hydrogen storage systems that are cost-effective, compact, flexible, and safe. To address this challenge, it is essential to establish distinct standards for hydrogen storage and fuel cell vehicles, catering to both stationary and mobile applications. The ideal hydrogen storage system must meet rigorous criteria, including safety, lightweight design, compactness, affordability, durability, long-term performance, and efficient refueling capabilities [6].

3 Climatic and environmental factors affecting producing green hydrogen

3.1 Panel degradation :

Panel degradation is the phrase used to describe the progressive deterioration of the PV system's properties, which may have an impact on its capacity to produce electricity. A panel is considered deteriorated when its power falls below 80% of its initial power, as recommended by the manufacturer. PV panel degeneration is caused by a number of conditions, including temperature, humidity, irradiation, and mechanical shock. The many causes of panel deterioration are shown in Table (I.2). Furthermore, hotspot creation is a problem since high temperatures have the potential to harm cells. Hotspot heating is caused by series-connected cells that are partially shadowed, broken, or misaligned. Research revealed a few techniques to reduce hotspots. Jerada et al. suggested a quick and precise hotspot identification method. Unwanted power generating losses can be eliminated with proper management of all these problems.

3.1.1 Dust characteristics, accumulation, and impact on PV module

Dust is a term used to describe materials that are suspended and dispersed by air, including particulate matter from burning fossil fuels, electric power, or motor vehicles and mechanisms, smoke from plants, kitchens, cars, and electric power plants, fog, and soil particles, which make up the majority of suspended dust in the air [17, 18]. Dust deposition on a PV panel is shown in figure (I.5). Additionally, inorganic materials from storms, factory smoke, forest fires, and

TABLEAU I.2 – Performance of PV module in partial shading conditions [13]

Conditions	**Area Shaded**	**Results**	**References**
Numerical simulation	2%	70% loss of energy	99
An arrangement of 33 cells of PV panel	Minimum loss : 24 half-shaded cells		
Maximum loss : 21 completely shaded cells	Power losses vary from 19% to 79%	100	
Non-transparent materials used for shading	25% solar radiation	Energy and exergy efficiencies are 7.28% and 5.74%, respectively, compared to 8.19% and 8.05% without shading	101
36 solar cells in various configurations	Partial shading : radiation varies from 0.85 to 1.01 kW/m^2	Highest peak power observed in TCT (total-cross-tied), SP (series-parallel), BL (bridge-linked), and HC (honeycomb) configurations	102
Shading from wall/-tree and seasonal variation	—	Energy loss of about 15% in winter and 1% in summer	103

volcanic gasses, as well as biological materials like bacteria and pollen, can form suspended airborne compounds. According to [18], some of these dust constituents include solid particles and tiny measurements that can float in the atmosphere for extended periods of time. concentrations. They also use wind movement to travel great distances from their source. The size, form, distribution, and concentrations of dust vary greatly, making it a complex category.Dust is a naturally occurring phenomenon that happens when a windstorm unexpectedly intensifies. This process causes the summer and winter atmospheric pressure systems to diverge significantly [19]. As wind speed rises and the sun's surface warms, the dust gets more intense. According to [20], dust follows the density of the type of land that travels through it or rose from, and its effects are not as frequent as those of other secondary variables like humidity, wind deviation, depressions, or air elevations.As the sun rises, its warm rays begin to reach the earth's surface, drying the soil and producing dust that is suspended in the atmosphere. Dust accumulates on items when the sun sets and the wind speed drops. Dust can occasionally increase in seasons other than the hot one because of the wind's strength or the place where it blows, which can happen on chilly winter days [21, 22] have studied the passive cooling of PV caused by overheating from

dust collection. However, from a technical and financial standpoint, air cooling was shown to be more promising. [23] also covered active cooling. In contrast to humid weather, the dryness of the atmosphere aids in generating dust [24]. When the rain stops and the vegetation covering the soil is eliminated, dust, a frequent phenomenon throughout the Middle East and North Africa, is abundant on the edges of deserts [25]. Countries impacted by the Mediterranean Sea climate have a different season from those impacted by the tropical wet summer. Dust storms are typically common in late spring and early summer in the first countries.

Fig. I.5 *Dust accumulation on PV panels [9].*

3.1.2 Influencing factors and consequences

Wind energy is the most developed type of renewable and "clean" energy from a techno-economic perspective. Of all the energy sources accessible today, wind-based renewable energy is regarded as an environmentally favorable option.Additionally, wind energy is thought to be the world's most suitable energy source for both humans and animals. In addition to offering several economic, social, and environmental advantages, it can efficiently adapt to climate change. A study by Cronin explains the causes of significant bird deaths linked to people in emerging nations. According to a calculation by the American Wind electricity Association, wind-based electricity can only result in one faunal death for every 250 bird deaths that are caused by humans. Impacts on wildlife have been noted by several researchers. While avoidable habitat degradation and displacement are indirect repercussions, mortality from a collision with a wind power station has direct ramifications. However, the impact is less than that of

other renewable energy sources.In order to lessen the negative consequences of wind energy on wildlife, industry and researchers are currently working to standardize preventive measures. Numerous academics have shown that a wind farm's appropriate placement can greatly lower avian mortality. According to reports, one of the biggest victims of wind turbine deaths globally is birds. Wind turbines kill very few birds, in contrast to other human activities. According to a study, just twenty out of the entire number of animals killed annually perished as a result of 1000 MW wind turbines, whereas the number of birds killed by hunters is counted. Approximately 1,500 people have died as a result of collisions with cars and electricity, and power transmission lines are nearly "invisible" to birds. In conclusion, it is critical to comprehend how wind turbines affect the ecosystem. In summary, we need to determine that it is preferable to construct power in a manner that has the least negative environmental impact if energy is to be generated. In both affluent and developing nations, raptors die at a significantly lower rate than birds and bats. One of the most common complaints during wind turbine installation is the threat posed by birds. According to studies, birds can become disoriented during inclement weather or on foggy evenings. The light from wind farms then attracts birds, which leads to more birds flying past wind power plants and becoming vulnerable due to collisions with wind turbine blades. It increases birds' ability to fly past wind turbine farms, particularly when there is enticing and charming color light present. In one investigation, only three out of 48 animals were discovered deceased when the weather was not a role.

3.1.3 Ecological influences : noise impact

Noise pollution is the most significant environmental effect of wind turbines. In order to safeguard participating and neighboring landowners from noise and safety hazards, turbines should be retracted from residential and property lines. There are two primary categories of noise produced by wind turbines : (1) aerodynamic noise and (2) mechanical noise. The distinctive "howling" sound produced by airflow above the turbine blades is known as aerodynamic noise. Sound insulation within the turbine casing or mechanical noise reduction at the design stage (side gears) are two options. During operation, the soundproofing curtain and the antivibration support feet can also help to reduce mechanical noise. Manufacturing companies can limit aerodynamic noise by properly designing the blades. In comparison to turbines, the erratic wind direction and speed tends to generate higher noise levels and ultimately result in the object being received. The wind turbine's bottom has higher noise levels, and the rotor's bottom

is situated between the factory and the receiving end. There is some noise produced by the turbine's mechanical components. A wind turbine located 350 meters away from a house is obviously not any noisier than a kitchen refrigerator. A schematic depiction of wind energy production and possible effects is shown in Figure (I.5).

3.1.4 Ecological influences : visual impact

The detrimental consequences of wind turbines have been assessed in terms of visual impact. Color contrast, size, distance from the house, flashing shadows, and time spent on the turbine are some of the visual effects that vary with wind energy equipment. Assessments based on Geographic Information Systems are frequently used to gauge visual impact. The breadth of the impacted region and the visual impact can be ascertained with the use of a Geographic Information System and visibility assessments when a specific site is recommended. The impacted area is referred to as the visual impact zone in conformity with contemporary planning rules. Plotting the degree of impact may be possible if the distance is taken into account and the degree of influence is set for the transmission line. According to certain reports, the more difference there is with the surrounding nature, the more of an impact wind turbines have. Actually, at the turbine's edge, designers frequently blend the turbine's pixels with the background pixels. When there are more pixels on the side, this impact becomes more noticeable at a larger distance. Regarding the visual and acoustic impact, the distance between the residential area and the wind turbine location is crucial. The installation of wind turbines and the distance between residential properties, especially farmhouses, have been restricted by authorities and laws. Various nations have implemented their own regulations that take into account the lives of the local residential properties. As the distance from the residential field increases, the turbine's visual impact diminishes.

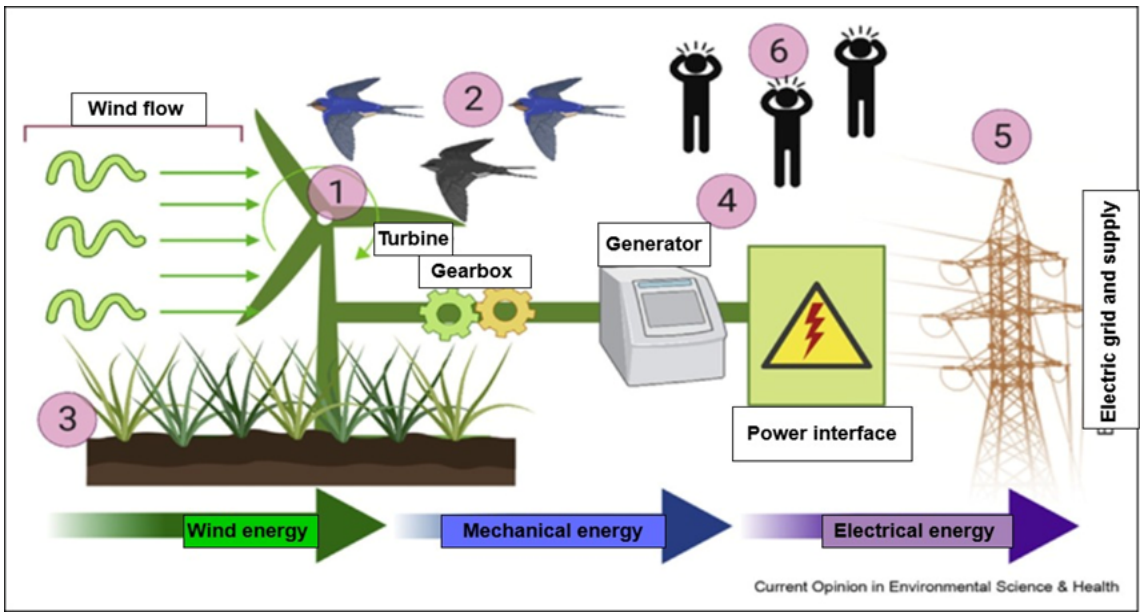

Fig. I.6 *Schematic representation of wind energy development and potential impacts, that is, (1) noise and visual, (2) bird fatality, (3) soil erosion and defor- estation, (4) lightening from towers, (5) electromagnetic, and (6) surrounding neighborhood.*

3.1.5 Ecological influences : soil erosion and deforestation .

Deforestation and soil erosion are two of the main ecological effects of wind energy farm growth. The local biological system is impacted by a number of operations, including the excavation of roads, foundations, and projected lands during the wind energy farm's construction. For example, removing plants from the ground causes unfavorable weather changes, such erratic rainfall patterns, which in turn cause soil erosion and other problems. Additionally, oil and wastewater from the building site have the potential to seep into the subsurface soil and pose major environmental issues. Areas with a lot of wind energy frequently have poor ecosystems and little biodiversity. The local ecological equilibrium may be upset by the erection of heavy machinery, and it may take a while for the environment to recover. According to China's wind turbine construction rules, excavation should be as labor-intensive as feasible in order to reduce interference from heavy machinery. Additionally, it should be advised to replace trees as soon as feasible following construction citenazir2020.

3.1.6 The dangers and effects of producing hydrogen :

The perception of safety surrounding hydrogen largely depends on the type of application involved. For instance, hydrogen refueling stations tend to be viewed as more hazardous compared to vehicles, particularly in contrast to gasoline stations and their vehicles. Notably, the primary

safety concerns revolve around the storage and transport of green hydrogen rather than its actual use in the transportation sector. In this context, worries about hydrogen safety are closely tied to the level of trust in the technology, which extends beyond mere communication strategies about this energy source. A case in point is Taiwan, where the confidence in the local industry and its adherence to safety standards significantly alleviates concerns, leading to minimal impact on the overall acceptance of hydrogen technologies. As a result, we can identify specific risk perceptions related to the safety of technologies associated with green hydrogen, particularly focusing on storage facilities, transportation methods, and pipeline usage. In this field, trust, technological accessibility, and the legitimacy of implementation play crucial roles in shaping perceptions of safety [26]. Addressing the economic and technical challenges associated with hydrogen storage and transport is essential for unlocking its full potential as an energy carrier. Numerous methods are available for storing hydrogen, each presenting its unique set of advantages and drawbacks [27] :

Table (I.3) of Advantages & Disadvantages of Green H2 Storage & Transportation

4 Case studies and existing renewable energy projects in the Algerian Sahara.

The RE master plan in Algeria focuses on the development of solar energy, with a total of 13,500 MW solar PV generation planned for 2030. The RE installed in Algeria based on technology is shown in Figure (I.6). Most of the installed PV in the country is aimed at providing electricity to rural areas with difficulties in grid extension. Figure (I.7) shows the locations of all PV stations in the country, and the list of installed PV farms is listed in Table (I.3).

Accessible by the end of 2019—with a combined capacity of 423 MW—seven times less than the goal of $3000MW$ by 2021 [23]. According to the initial target, a total of 60 PV generation plant projects were planned for the period 2011 to 2020 [2].

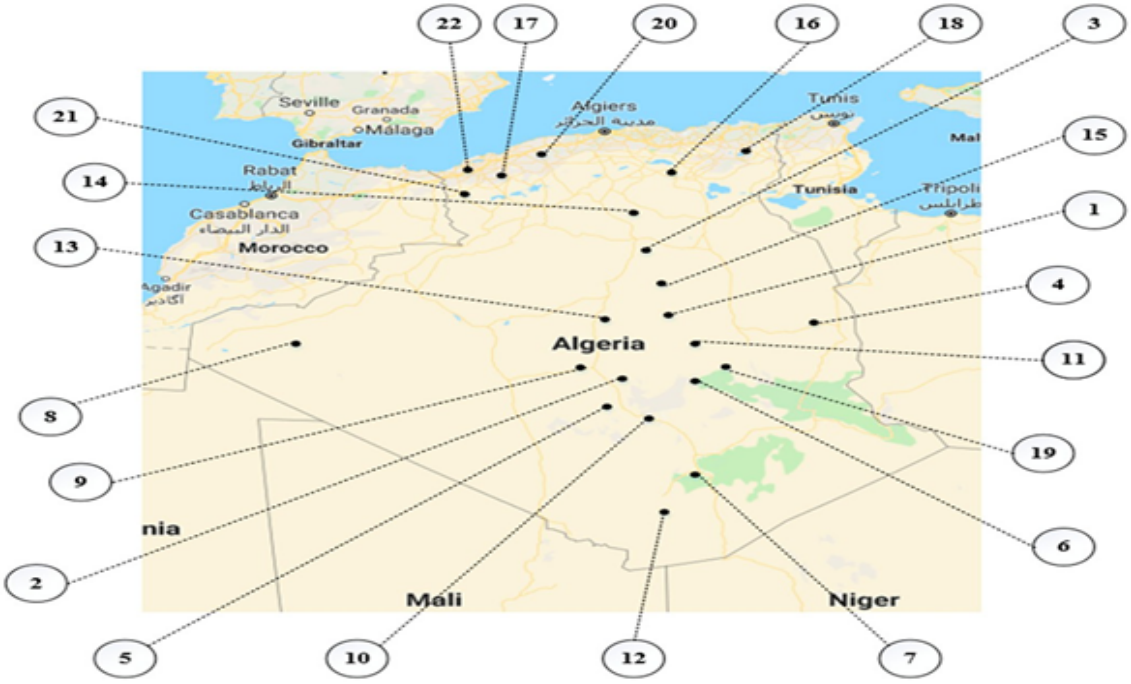

Fig. I.7 *Locations of PV stations in Algeria.*

TABLEAU I.3 – List of Solar Power Stations in Algeria (Split View)

No.	Station	Location	MW	No.	Station	Location	MW
1	SPP1	Hassi R'mel	25	12	In Salah	Tamanrasset	5
2	SPE	Adrar	10	13	Aoulef	Adrar	5
3	Ghardaïa	Ghardaïa	11	14	Ain El-Ibel	Djelfa	20
4	Djanet	Illizi	3	15	Khang	Laghouat	20
5	Adrar	Adrar	20	16	Oued El-Kebrit	Souk Ahras	15
6	Kabertene	Adrar	13	17	Sedrate Leghzal	Naâma	20
7	Tamanrasset	Tamanrasset	13	18	Ain El-Melh	M'sila	20
8	Tindouf	Tindouf	9	19	El-Hadjira	Touggourt	10
9	Z. Kounta	Adrar	6	20	Ain Shouna	Saïda	30
10	Timimoun	Adrar	9	21	E.B.S Chikh	El Bayadh	24
11	Reggane	Adrar	5	22	Telga	Tlemcen	12

4.1 wind Kaberten

(Kaberten) 10 MW wind turbine power plant Installed in the Kaberten region, the farm depicted in figure (I.8) relies on wind energy and produces electrical energy using Doubly Fed Induction Generators (DFIG), which are made by GAMESA and have a combined nominal output of 0.85 MW, producing 690 Vac. The station, which spans 33 hectares and is connected to the 30 kV PIAT electrical distribution network, is made up of twelve (12) wind turbines with a combined 10 MW of output. Each turbine is connected to the others in parallel to make maintenance easier. Each of these turbines can cut greenhouse gas emissions by 1000 tons year.

Fig. I.8 *Panoramic photograph of the 10 MW wind turbine farm (Kaberten) [5].*

5 Conclusion

In short, the Algerian Sahara is extremely promising for the production of green hydrogen, facilitated by abundant solar and wind power resources and the availability of water resources—limited though they may be—whose optimal management is possible through advanced technologies such as water recycling and desalination. The extensive, uninhabited area of the region combined with high solar irradiance levels makes the area especially suitable to the large-scale use of renewable energies. The application of green hydrogen in mobility provides a credible pathway to decarbonize, especially in heavy and long-distance mobility, where conventional electric solutions remain limited. However, the production and use of green hydrogen in the

Sahara are subjected to a range of climatic and environmental factors such as severe heat, dust loading, and water scarcity, which must be managed through utilized technical and operational solutions. Finally, After outlining the enormous potential and difficulties of producing green hydrogen in the Algerian Sahara, the following chapter will examine the technical elements that are essential to its success. In addition to analysing regionally specific renewable energy profiles to maximise the integration of solar and wind power into the hydrogen production process, we will concentrate on modelling electrolysers to comprehend their performance and efficiency under various conditions. The foundation for creating efficient and long-lasting green hydrogen systems will be laid by this thorough analysis.

Chapter II

Components modelling electrolyzer and renewable energy profiles

1 Introduction

Green hydrogen is a crucial part of the world's energy systems of the future. It is created byelectrolyzing water with renewable energy. We present a selection of reviews on some of the major research topics pertaining to the comprehension of the fundamental processes and component design in both existing and developing water-electrolysis technologies in this themed issue of Chemical Reviews.Low carbon emissions are produced by producing green hydrogen through water electrolysis driven by renewable energy sources like solar, wind, or hydropower, or perhaps nuclear energy [28]. Among ,the various technologies available for hydrogen generation, Proton Exchange Membrane (PEM) electrolyzers have emerged as a promising solution due to their high efficiency, fast dynamic response, and ability to produce high-purity hydrogen. PEM electrolyzers function by splitting water molecules into hydrogen and oxygen using electrical energy, making them particularly suitable for integration with intermittent renewable sources such as solar or wind power. To ensure optimal operation of a PEM electrolyzer, especially when powered by variable renewable sources, power electronics and control systems play a crucial role. The integration typically involves a DC-DC boost converter regulated by a Maximum Power Point Tracking (MPPT) algorithm to extract maximum energy from sources like photovoltaic panels. Additionally, an AC-DC converter is often required to interface with grid-connected systems or other AC power sources. This chapter focuses on the modeling and of hydrogen production using a PEM electrolyzer, along with the modeling of the associated power electronics converters. The first part delves into the physical and electrochemical principles of the PEM electrolyzer and its mathematical modeling for simulation purposes. The second part addresses the design and control of the MPPT-based DC-DC boost converter, which ensures that the maximum available power is delivered to the electrolyzer. Lastly, the modeling of an AC-DC converter is presented, highlighting its role in maintaining power quality and efficient energy conversion in hybrid systems.Through comprehensive modeling, this chapter aims to provide a foundation for designing efficient, renewable-powered hydrogen production systems.

2 The principle of water electrolysis :

Water electrolysis involves passing a direct current (DC) between two electrodes immersed in an electrolyte solution to decompose water (H_2O). This process results in the formation of

hydrogen gas (H_2) at the cathode and oxygen gas (O_2) at the anode. The amount of hydrogen produced is directly proportional to the electrical current applied to the electrodes.

In recent years, there has been a growing interest in using electrolysers for the production of green hydrogen—hydrogen generated from renewable energy sources such as solar or wind power. Water electrolysis is a key technology for producing this environmentally friendly hydrogen, offering a clean alternative to fossil-fuel-based methods.

Electrolysers are the devices that carry out this transformation. They function by splitting water molecules (H_2O) into their elemental components—hydrogen and oxygen—through the application of DC electricity. While there are different types of electrolysers, which will be discussed further below, they all operate based on the same overall chemical reaction :

$$\mathrm{H_2O} \rightarrow \mathrm{H_2(g)} + \frac{1}{2}\mathrm{O_2(g)} \tag{II.1}$$

The electrolysis process takes place within an electrolytic cell, which is composed of three essential components : two electrodes (the cathode and the anode) and an electrolyte (which can be either a liquid or a solid, depending on the technology used). The electrolyte facilitates the transfer of ions between the electrodes, enabling the water-splitting reaction.

Electrolyser technologies are continuously evolving, and various types are available on the market—each offering distinct advantages and limitations. These technologies differ in the materials used and the specific electrochemical reactions occurring at the anode and cathode, although they all share the same overall water-splitting reaction.

— **Low Temperature Electrolysers (LTE)** : Operate at temperatures below 100 °C, using liquid water as the feedstock.

— **High Temperature Electrolysers (HTE)** : Operate at elevated temperatures, typically in the range of $400 - -1000\,\check{\mathrm{r}}C$, and use steam instead of liquid water.

Another method of classification is based on the **Technology Readiness Level (TRL)**, which assesses the maturity of a technology for practical applications. This framework helps identify which electrolyser technologies are most developed and ready for deployment across different use cases [29].

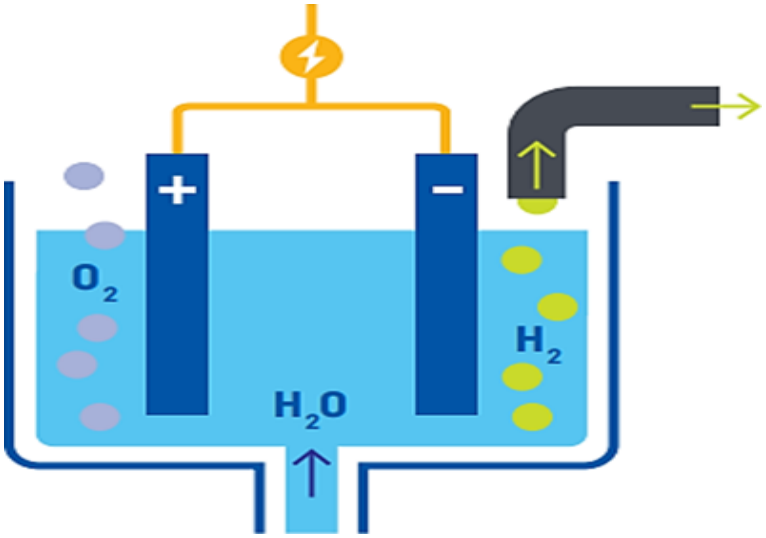

Fig. II.1 *The schematic procedure for Green Hydrogen production [6].*

Figure (II.1) illustrates a comparative chart of various electrolyzers used for hydrogen production. The purpose of this diagram is to highlight the primary features of each type of electrolyser, assisting in the decision-making process regarding technology selection based on specific operational requirements and constraints.

The diagram distinguishes four main types of electrolysers, summarized as follows :

— **Alkaline Electrolyzer (AEL)** : Operates between 60 °C and 80 °C, with efficiency ranging from 65% to 82%. It uses an alkaline electrolyte such as potassium hydroxide (KOH) or sodium hydroxide (NaOH). AEL is a well-established and proven technology, but its low current density limits its compatibility with intermittent renewable energy sources.

— **Proton Exchange Membrane Electrolyzer (PEM)** : Functions at temperatures between 50 °C and 80 °C, achieving an efficiency of 70% to 85%. It utilizes a solid polymer electrolyte membrane. PEM electrolysers offer high current density and fast dynamic response, but they are costly and require high-purity water.

— **Solid Oxide Electrolyzer (SOE)** : Operates at high temperatures ranging from 700 °C to 1000 °C, with the highest efficiency among all, approximately 85% to 90%. It uses a solid ceramic as the electrolyte. While SOE provides excellent efficiency and allows heat recovery, it suffers from a limited service life and is still in the development stage.

— **Anion Exchange Membrane Electrolyzer (AEM)** : Works at moderate temperatures between 40 °C and 60 °C, with efficiencies from 65% to 75%. It employs an anion-conductive

polymer membrane. Although still not fully commercialized, AEM offers promising potential for low-cost hydrogen production in the future.

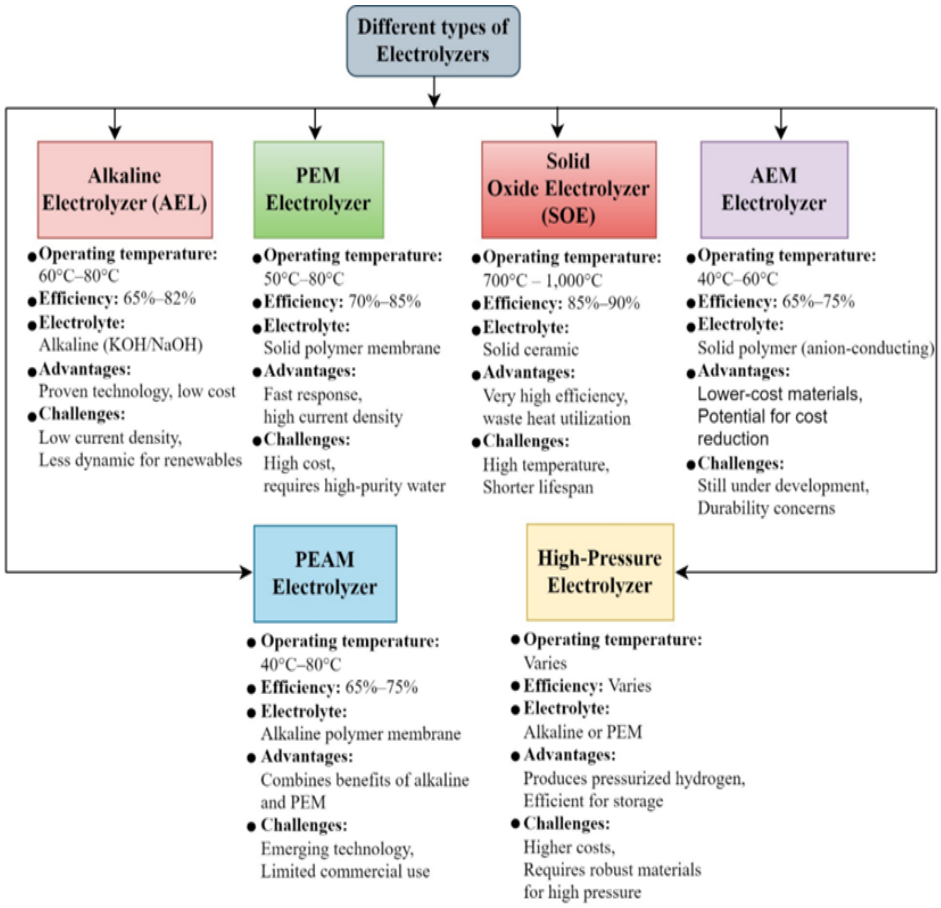

Fig. II.2 *Classification and comparison of electrolyzer gypes for hydrogen production.*

We employed a proton exchange membrane (PEM) electrolyzer in this investigation since it isamong the most advanced and widely utilized . Be. In addition to producing hydrogen at a pressure of 1.2 bar, which enables the hydrogen to be stored immediately without the need for compression, PEM offers high efficiency, life cycle, and adaptability with the fluctuations of power generation loads from renewable energy [30].

2.1 Electrolysis of Proton Exchange Membrane (PEM)

The PEM water electrolysis schematic diagram is displayed in Figure (II.3). Electricity is used as the energy source in the endothermic process of electrolysis. It is thermodynamically possible for the water electrolysis reaction to occur at potentials greater than 1.23 V vs. RHE (reversible hydrogen electrode). 1.48 V vs. RHE is the thermoneutral potential at which the cell can function adiabatically. Heat is produced by the reaction in typical PEM water electrolysis

devices, which run at potentials well over 1.48 V vs. RHE. A solid polymer electrolyte (Nafion) with a thickness of less than 0.2 mm separates the anode and cathode of the PEM water electrolysis system, much like in a proton exchange membrane fuel cell (PEMFC). Protons, electrons, and oxygen are produced at the anode during the oxidation of water. To be reduced to hydrogen, the protons are transferred across the electrolyte membrane. Iridium is commonly used as a catalyst for oxygen evolution or water oxidation because of its high anode overpotential, which allows it to withstand corrosive environments. A titanium flow field channels water to the anode, and a section of porous titanium mesh acts as a diffusion layer between the water channel and the anode catalyst layer. The cathode configuration is similar to the PEMFC with Pt-based catalyst and a graphite flow field to transport hydrogen. A piece of carbon paper is used as the gas diffusion layer (GDL) placed between the cathode catalyst and the flow field. With a graphite flow field to transport hydrogen and a Pt-based catalyst, the cathode configuration is comparable to the PEMFC. The gas diffusion layer (GDL), which is positioned between the cathode catalyst and the flow field, is made of a piece of carbon paper. According to Faraday's law, the rate at which hydrogen is produced in an ideal electrolysis is proportional to the charge transferred. It is able to be stated as :

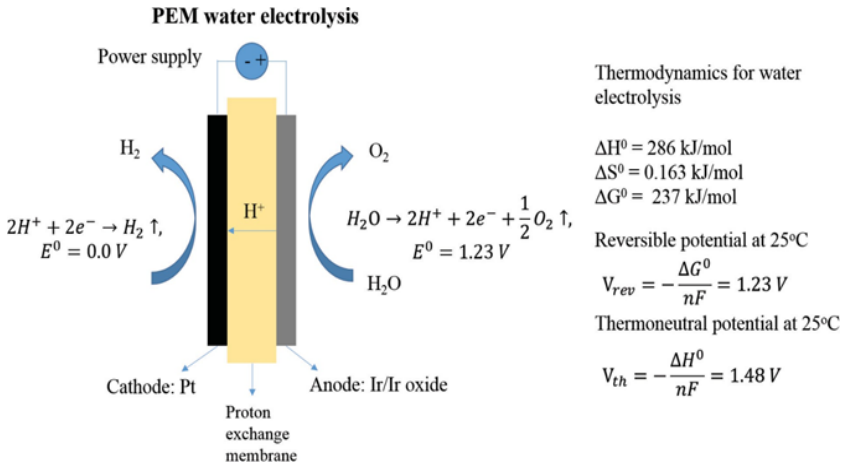

Fig. II.3 *Schematic diagram of PEM water electrolysis and the fundamental thermodynamic properties [7].*

2.1.1 PEM Electrolyser Validation and Modeling

An electrolyser's polarization curve which illustrates the relationship between current density and cell voltage is its primary performance indicator [31]. This relationship is defined by equation ((II.2)) :

$$V = N_C \cdot (E_{OCV} + V_{\text{act},a} + V_{\text{act},c} + V_{\text{ohm}}) \tag{II.2}$$

Where :

— N_C is the number of cells in the electrolyser,

— E_{OCV} is the open circuit voltage (V),

— $V_{\text{act},a}$ and $V_{\text{act},c}$ are the activation overpotentials at the anode and cathode respectively (V),

— V_{ohm} is the ohmic overpotential (V).

At high current densities, additional voltage losses due to concentration effects may occur. These losses arise when the abundance of reacting species slows down the reaction rate. However, in PEM electrolysers, such losses are negligible until current densities reach approximately 1.6 A/cm^2. Therefore, this value is chosen as the upper limit for modeling to balance efficiency and hydrogen production.

The open circuit voltage is calculated using the Nernst equation [31] (Equation (II.3)) :

$$E_{OCV} = E_{rev} + \frac{R \cdot T}{n \cdot F} \cdot \ln\left(\frac{P_{H_2} \cdot P_{O_2}}{P_{H_2O}}\right) \tag{II.3}$$

Where :

— $P_{H_2}, P_{O_2}, P_{H_2O}$ are the partial pressures of hydrogen, oxygen, and water (Pa),

— T is the temperature (K),

— R is the universal gas constant (J/mol $\cdot$ K),

— F is Faraday's constant (C/mol),

— E_{rev} is the reversible cell potential (V).

The reversible potential E_{rev} is determined using the empirical relation (Equation (II.4)) :

$$E_{rev} = 1.229 - 0.9 \times 10^{-3} \cdot (T - 298)^2 \tag{II.4}$$

We assume that the liquid water in the cell exerts a partial pressure equivalent to its saturated vapor pressure at temperature T, and that both anode and cathode operate at atmospheric pressure.

The activation overpotentials are modeled using the Tafel equation, derived from the Butler-Volmer expression :

$$V_{\text{act},x} = \frac{R \cdot T}{n \cdot F \cdot \alpha_x} \cdot \ln\left(\frac{i}{i_{0,x}}\right) \tag{II.5}$$

Where :

— α_x is the charge transfer coefficient for electrode x (anode or cathode),

— i is the current density (A/cm^2),

— $i_{0,x}$ is the exchange current density (A/cm^2),

and $i_{0,x}$ is obtained via the Arrhenius equation using reference current density and activation energy.

Ohmic overpotential is calculated via Ohm's law, taking into account the membrane resistance :

$$V_{\text{ohm}} = \frac{\delta}{\sigma \cdot i} \tag{II.6}$$

Where :

— δ is the membrane thickness (m),

— σ is the membrane conductivity (S/m), determined using an Arrhenius-based model with σ_{ref} and E_{pro}.

The hydrogen production rate is calculated using Faraday's law (Equation (II.7)) :

$$\dot{n}_{H_2} = \frac{\eta_f \cdot i \cdot A_{\text{cell}} \cdot N_C}{2 \cdot F} \tag{II.7}$$

Where :

— A_{cell} is the active area of a single cell (m^2),

— η_f is Faraday's efficiency (assumed 100% in this model).

The electrical power consumed by the electrolyser is given by :

$$P_{el} = V \cdot i \cdot A_{\text{cell}} \cdot N_C \tag{II.8}$$

Finally, the energy efficiency (conversion of electricity into hydrogen energy [7]) is expressed as :

$$\eta = \frac{P_{out}}{P_{in}} = \frac{\dot{m}_{H_2} \cdot HHV}{P_{el}} \tag{II.9}$$

where HHV is the higher heating value of hydrogen, and $\dot{m}_{H_2}$ is the mass flow rate of produced hydrogen.

2.1.2 Resistive model

The electrolyzer is represented as a voltage source, which represents the reversible potential, and an electrical resistance in series, which explains the ohmic losses, in the simplest circuit (Figure (II.4)). It could be represented in this manner because, throughout the majority of the polarization curve's range, the voltage to current ratio can be regarded as constant

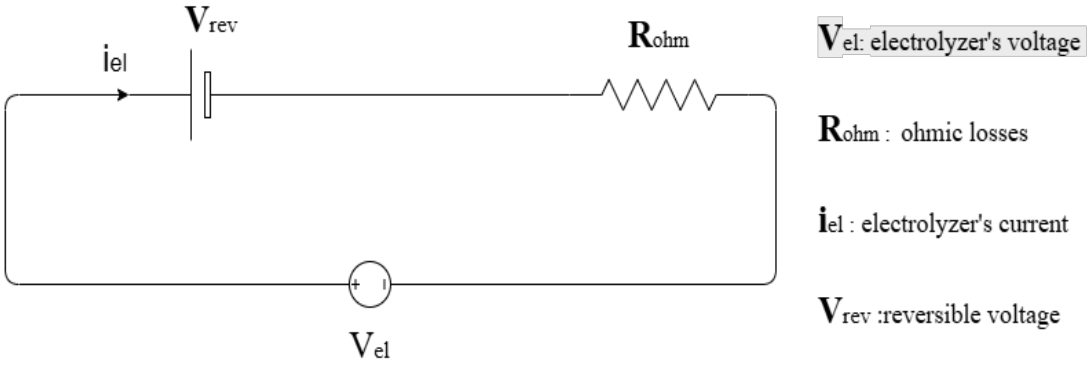

Fig. II.4 *Resistive equivalent circuit for a PEMEC.*

Despite being a simple model, the findings are satisfactory. However, because the model ignores temperature and pressure, voltage and resistance must be determined empirically using the polarization curve and computed for each pair of variables.

2.1.3 Dynamic model

When the system's dynamics are taken into consideration, the accuracy increases. It presents the electric double layer (EDL) effect, which is the presence of a potential difference in the electrode-electrolyte interface even in the absence of current flow. This is modeled as a capacitor and results from the adsorption of ions on the electrode surface that are separated from the electrode by an insulating gap.

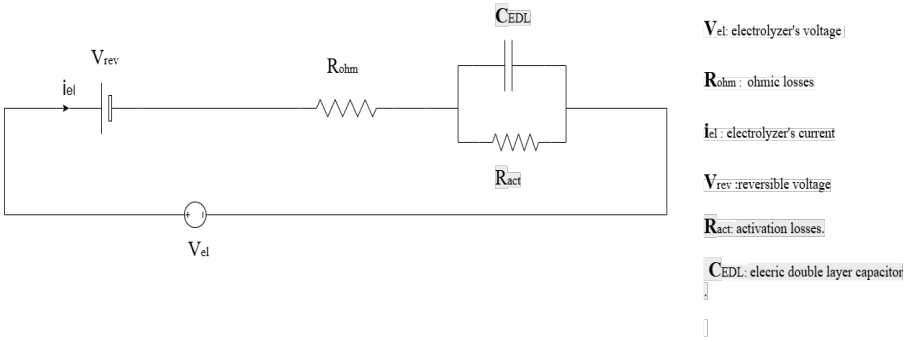

Fig. II.5 *Dynamic equivalent circuit for a PEMEC.*

A resistance for the ohmic losses in series with a resistance for the activation overpotentials in parallel with the EDL capacitor, as shown in Figure 5, conforms the entire system to the reversible voltage in series with a Randles cell .

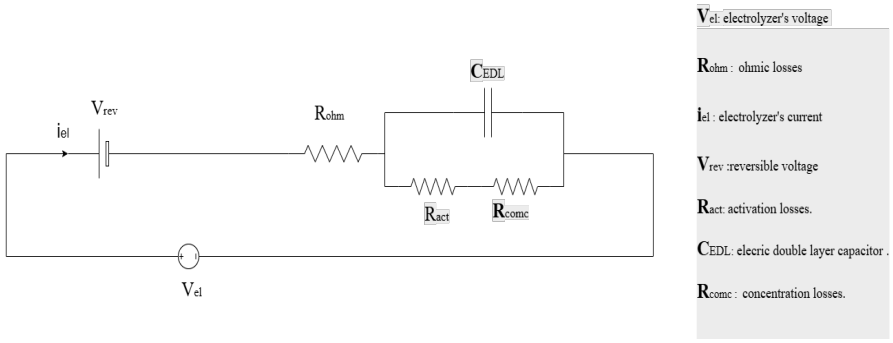

Fig. II.6 *Dynamic equivalent circuit for a PEMEC [8].*

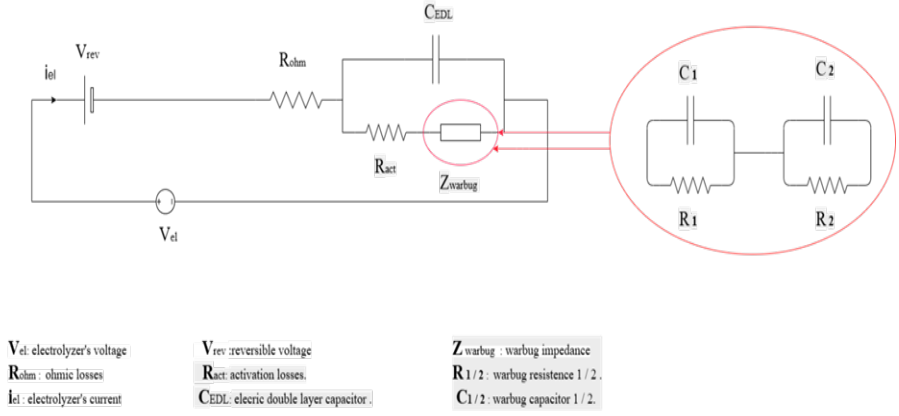

Fig. II.7 *Electrochemical model without the activation overpotential of the cathode and with Randles–Warburg impedance [9].*

This model describes the cell voltage across a PEM stack in the absence of the activation overpotential at the cathode. The relationship is given by Equation (II.10) :

$$V_{el} = V_{\text{act},a} + R_{\text{ohm}} \cdot i_{el} + V_{rev} \tag{II.10}$$

where :

— V_{el} is the cell voltage,

— $V_{\text{act},a}$ is the activation overpotential at the anode,

— R_{ohm} is the ohmic resistance,

— i_{el} is the cell current density,

— V_{rev} is the reversible voltage.

The dynamic behavior of the activation overpotential at the anode is modeled using a simplified differential equation (Equation (II.11)) :

$$\frac{dV_{\text{act}}}{dt} = \frac{i_{\text{cell}}}{C_{\text{edl}}} - \frac{V_{\text{act}}}{(R_{\text{act}} + Z_{\text{Warburg}}) \cdot C_{\text{edl}}} \tag{II.11}$$

where :

— C_{edl} is the double-layer capacitance,

— R_{act} is the charge transfer resistance,

— Z_{Warburg} is the Warburg impedance (used to model mass transport),

— i_{cell} is the cell current.

This model represents a classical electrochemical formulation and can also be simplified by neglecting the Warburg impedance in certain conditions. The voltage behavior across the PEM cell stack as predicted by this model is consistent with the electrochemical principles outlined in [**?**].

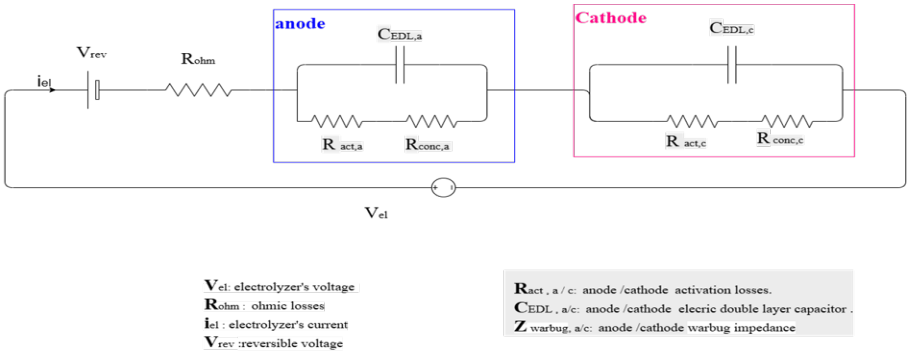

Fig. II.8 *Dynamic equivalent circuit used for PEMEC accounting for the ohmic + activation + concentration losses as a resistance, divided into anode and cathode contributions [21]..*

The full expression for the cell voltage across a PEM electrolyser, including both activation overpotentials and ohmic losses, is given by Equation II.12 :

$$V_{el} = V_{\text{act},c} + V_{\text{act},a} + R_{\text{ohm}} \cdot i_{el} + V_{\text{rev}} \tag{II.12}$$

Where :

— i_{el} is the input current to the electrolyser (A),

— R_{ohm} is the ohmic resistance (Ω),

— V_{rev} is the reversible potential (V),

— $V_{\text{act},a}$ and $V_{\text{act},c}$ are the activation overpotentials at the anode and cathode, respectively (V).

The dynamic behavior of the activation overpotentials is governed by the following differential equations :

$$\frac{dV_{\text{act},c}}{dt} = \frac{i_{\text{cell}}}{C_{\text{edl},c}} - \frac{V_{\text{act},c}}{R_{\text{act},c} \cdot C_{\text{edl},c}} \tag{II.13}$$

$$\frac{dV_{\text{act},a}}{dt} = \frac{i_{\text{cell}}}{C_{\text{edl},a}} - \frac{V_{\text{act},a}}{R_{\text{act},a} \cdot C_{\text{edl},a}} \tag{II.14}$$

Where :

— $R_{\text{act},a}$ and $R_{\text{act},c}$ are the temperature-dependent charge transfer resistances at the anode and cathode (Ω),

— $C_{\text{edl},a}$ and $C_{\text{edl},c}$ are the double-layer capacitances (F),

— i_{cell} is the total cell current (A).

Randles–Warburg Model : When diffusion effects are considered (e.g., for mass transport limitations), the cathodic overpotential includes the Warburg impedance term. The corresponding expression becomes :

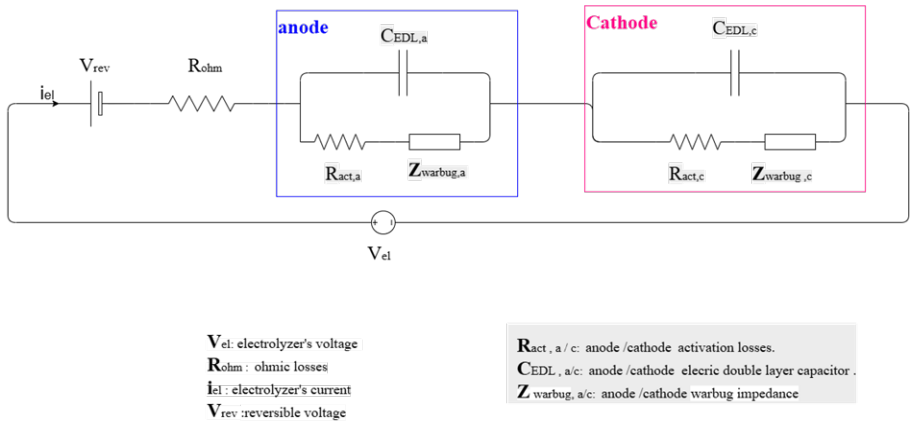

Fig. II.9 *Dynamic equivalent circuit used for PEMEC accounting for the ohmic + activation + concentration losses as a Warburg impedance, divided into anode and cathode contributions[21].*

$$\frac{dV_{\text{act},c}}{dt} = \frac{i_{\text{cell}}}{C_{\text{edl},c}} - \frac{V_{\text{act},c}}{(R_{\text{act},c} + Z_{\text{Warburg}}) \cdot C_{\text{edl},c}} \tag{II.15}$$

This formulation represents a classical electrochemical model enhanced by the Randles–Warburg equivalent circuit, capturing both kinetic and mass transport effects [**?**].

$$\frac{dV_{\text{act},c}}{dt} = \frac{i_{\text{cell}}}{C_{\text{edl},c}} - \frac{V_{\text{act},c}}{(R_{\text{act},c} + Z_{\text{Warburg}})C_{\text{edl},c}} \tag{II.16}$$

$$\frac{dV_{\text{act},a}}{dt} = \frac{i_{\text{cell}}}{C_{\text{edl},a}} - \frac{V_{\text{act},a}}{(R_{\text{act},a} + Z_{\text{Warburg}})C_{\text{edl},a}} \tag{II.17}$$

where Z_{Warburg} stands for the frequency-dependent Warburg impedance. It is expressed mathematically as :

$$Z_{\text{Warburg}} = \frac{R_1}{1 + R_1 C_1} + \frac{R_2}{1 + R_2 C_2} \tag{II.18}$$

2.1.4 Electrochemical model

In order to develop a more specific relationship between voltage and current, it is first necessary to provide a thorough description of the chemical interactions that take place within the cell and the other components of the system. Only the membrane's characteristics and the electrocatalysts being used affect the model[32, 31]. Equation (II.19), where we can differentiate between the reversible voltage, the Faradaic losses, which correspond to the activation potential, and the non-Faradaic losses, which are associated with the ohmic and concentration potentials, already describes the primary

$$V_{\text{cell}} = V_{\text{rev}} + V_{\text{act}} + V_{\text{con}} + V_{\text{ohm}} \tag{II.19}$$

contributions to the voltage drop in the PEMEC. Both temperature and pressure have an impact on the reversible voltage's value. It is frequently expressed using the Nernst formula, as shown in Equation (II.19) :
The contributions to the voltage drop in the PEMEC are mainly due to reversible, activation, concentration, and ohmic losses.

Both temperature and pressure have an impact on the reversible voltage value. It is frequently expressed using the Nernst equation, as shown in Equation (II.20) :

$$V_{\text{rev}} = V_{\text{rev},T} + \frac{RT}{zF} \ln\left(\frac{P_{H_2} \cdot P_{O_2}^{1/2}}{P_{H_2O}}\right) \tag{II.20}$$

The reversible voltage $V_{\text{rev},T}$ previously mentioned can also be determined from the Gibbs free energy as :

$$V_{\text{rev}} = \frac{\Delta G_R}{zF} \tag{II.21}$$

Equation (II.22) provides the activation overpotential, including the contributions from both electrodes, based on the Butler–Volmer equation :

$$V_{\text{act}} = \frac{RT}{\alpha_{\text{an}} F} \sinh^{-1}\left(\frac{I_{\text{cell}}}{2i_{0,\text{an}}}\right) + \frac{RT}{\alpha_{\text{cat}} F} \sinh^{-1}\left(\frac{I_{\text{cell}}}{2i_{0,\text{cat}}}\right) \tag{II.22}$$

The concentration overpotential, associated with mass transport limitations, is described by :

$$V_{\text{con}} = \frac{RT}{4F} \ln\left(\frac{C_{O_2}}{C_{O_2O}}\right) + \frac{RT}{2F} \ln\left(\frac{C_{H_2}}{C_{H_2O}}\right) \tag{II.23}$$

Finally, the ohmic losses follow Ohm's law, accounting for internal resistance of the membrane and interface layers :

$$V_{\text{ohm}} = I_{\text{cell}} \cdot R_{\text{ohm}} = I_{\text{cell}} \cdot (R_{\text{membrane}} + R_{\text{interfaces}}) \tag{II.24}$$

The membrane resistance is expressed as :

$$R_{\text{membrane}} = \frac{\delta}{\sigma A} \tag{II.25}$$

Where :

— δ is the membrane thickness (m),

— σ is the ionic conductivity of the membrane (S/m),

— A is the active membrane area (m^2).

3 athematical Model of PV Power Generation :

To accurately establish the mathematical model of a photovoltaic (PV) cell and facilitate subsequent analysis, we assume that the current generated by the photoelectric effect remains constant when the irradiance is stable. This allows us to represent the PV cell as an ideal current source with a current value denoted as Iph. The equivalent circuit of the photovoltaic module is illustrated in Figure10. The derivation of the mathematical model follows these principles [33, 34, 35](Aouali et al. , 2014 ; Dey et al. , 2016 ; Chandel et al. , 2019) :

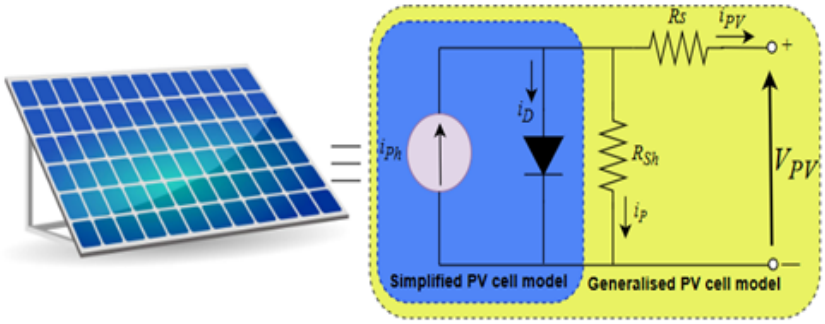

Fig. II.10 *The PV cell's equivalent circuit.*

According to Kirchhoff's Current Law (KCL) :

$$I = I_{\text{ph}} - I_d - I_{\text{sh}} \tag{II.26}$$

where I_{ph} represents the photo-generated current, I_d is the diode (P-N junction) current, and I_{sh} is the current through the shunt resistor R_{sh}, all measured in amperes (A).

The diode current and voltage relation is given by :

$$I_d = I_0 \left(e^{\frac{q}{MKT}(U+IR_s)} - 1 \right) \tag{II.27}$$

where :

— I_0 is the diode reverse saturation current (A),

— q is the elementary charge of an electron (C),

— M is the ideality factor of the diode (typically ≈ 1),

— K is the Boltzmann constant (1.38×10^{-23} J/K),

— T is the absolute temperature (K),

— U is the voltage across the cell (V),

— R_s is the series resistance (Ω).

According to Kirchhoff's Voltage Law (KVL), the current through the shunt resistor is :

$$I_{\text{sh}} = \frac{U + IR_s}{R_{\text{sh}}} \tag{II.28}$$

Substituting Equations (II.27) and (II.28) into Equation (II.26) yields :

$$I = I_{\text{ph}} - I_0 \left(e^{\frac{q}{MKT}(U+IR_s)} - 1 \right) - \frac{U + IR_s}{R_{\text{sh}}} \tag{II.29}$$

Since R_{sh} is large and R_s is small, the term $\frac{U+IR_s}{R_{\text{sh}}}$ can be neglected. Considering $I_{\text{ph}} = I_{\text{sc}}$, the formula simplifies to :

$$I = I_{\text{sc}} \left[1 - B\left(e^{\frac{U}{CU_{\text{OC}}}} - 1\right)\right] \tag{II.30}$$

Here, U_{OC} is the open-circuit voltage (when $I = 0$, $U = U_{\text{OC}}$), and at the maximum power point ($U = U_m$, $I = I_m$), the relation becomes :

$$I_m = I_{\text{sc}} \left[1 - B\left(e^{\frac{U_m}{CU_{\text{OC}}}} - 1\right)\right] \tag{II.31}$$

From Equation (II.31), at room temperature, one can deduce :

$$B = \left(1 - \frac{I_m}{I_{\text{sc}}}\right) e^{-\frac{U_m}{CU_{\text{OC}}}} \tag{II.32}$$

Tableau II.1 – Parameter values

Parameter	**Value**	**Parameter**	**Value**
T_{ref}	25 °C	B	0.5
s_{ref}	1000 W/m^2	C	0.00288/°C
A	0.0025/°C		

According to the set open circuit condition, substituting into Eq. (II.31) yields :

$$0 = I_{SC} \left[1 - \left(1 - \frac{I_m}{I_{sc}}\right) e^{-\frac{U_m}{CU_{OC}} e^{\frac{1}{C}}} - 1\right] \tag{II.33}$$

Since $e^{1/C} - 1$ is much greater than 0, then :

$$C = \left(\frac{U_m}{U_{oc}} - 1\right) \left[\ln\left(1 - \frac{I_m}{I_{sc}}\right)\right]^{-1} \tag{II.34}$$

Because environmental factors in real-world applications cannot be considered fixed, the operation of PV cells is influenced by changes in surrounding conditions. Therefore, adjustments to environmental parameters are necessary to approximate real working environments [**?**]. The correction scheme is as follows :

$$\Delta t = t - t_{\text{ref}} \tag{II.35}$$

$$\Delta s = \frac{s}{s_{\text{ref}}} - 1 \tag{II.36}$$

$$\hat{I}_{sc} = I_{sc}\left(\frac{s}{s_{\text{ref}}}\right)(1 - a\Delta t) \tag{II.37}$$

$$\hat{U}_{sc} = U_{sc}\left[1 - c\Delta t \ln\left(e - b\Delta s\right)\right] \tag{II.38}$$

$$\hat{I}_{m} = I_{m}\left(\frac{s}{s_{\text{ref}}}\right)(1 - a\Delta t) \tag{II.39}$$

$$\hat{U}_{m} = U_{m}\left[1 - c\Delta t \ln\left(e - b\Delta s\right)\right] \tag{II.40}$$

where t_{ref} and s_{ref} represent the reference temperature and irradiance, respectively. The correction factors are a, b, and c. Table (II.1) displays the precise values of these parameters [**?**].

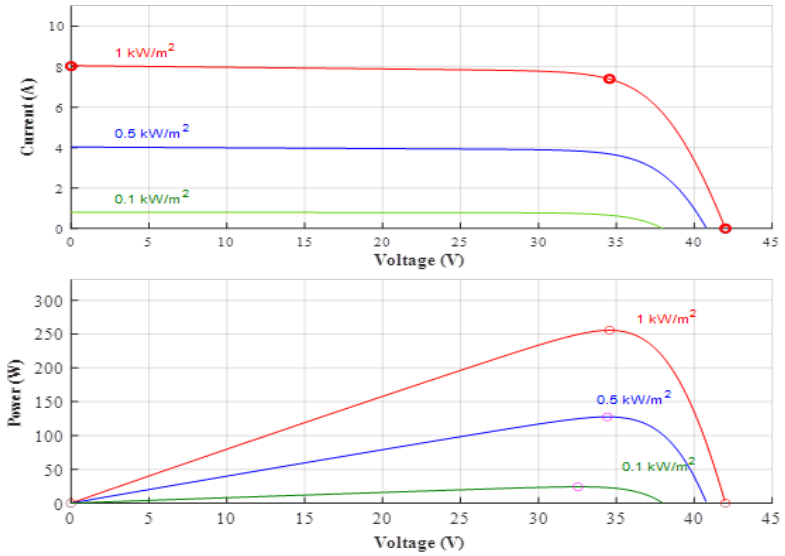

Fig. II.11 *Characteristics of the PV cell at different illumination levels : (a) current/voltage characteristic, (a) power/voltage characteristic.*

The figure represents the current-voltage (I-V) and power-voltage (P-V) characteristics of the PV module for different levels of illumination at a constant temperature ($T = 25\check{r}C$). It can be observed that the short-circuit current (Isc) varies proportionally with irradiation, whereas the open-circuit voltage (Voc) remains nearly constant. Additionally, the power curves exhibit distinct optimal points, which correspond to the maximum power points (MPP) under varying irradiation levels for a fixed temperature.

4 DC-DC Boost Converter Modeling

Mathematical models of DC-DC converters are discussed in [41,42]. Assuming ideal converter components and operation in continuous conduction mode (CCM), the state-space equations of the boost converter are derived. The duty cycle (D) for both SW_{ON} and SW_{OFF} modes is expressed over the entire switching period (T). The governing equations, as presented in [31, 36], are as follows :

When the switch (SW) is turned ON,

$$\begin{cases} \dfrac{dI_L}{dt} = \dfrac{1}{L}V_s \\ \dfrac{dV_0}{dt} = \dfrac{1}{C}(-V_0RT) \end{cases} \quad ; \quad 0 < t < T, \text{ SW on} \tag{II.41}$$

Similarly, when the switch SW is OFF,

$$\begin{cases} \dfrac{dI_L}{dt} = \dfrac{1}{L}V_s \\ \dfrac{dV_0}{dt} = \dfrac{1}{C}(-V_0RT) \end{cases} \quad ; \quad 0 < t < T, \text{ SW on} \tag{II.42}$$

4.1 Boost converter

The output voltage of this step-up converter is higher than the source voltage. Figure 12. The DC source is connected in series with an inductor.A MOSFET linked across the source functions as a switch. Both the source and inductor voltages are added while the switch is in the off position.As a result, the load voltage is rising above the source. When switch Q closes, energy is stored in the inductor, and when it opens, the energy is released. The pulse width modulation (PWM) technique is used to achieve duty cycle variation. Consequently, the diode will charge the capacitor since the two sources will be connected in series, creating a higher voltage.

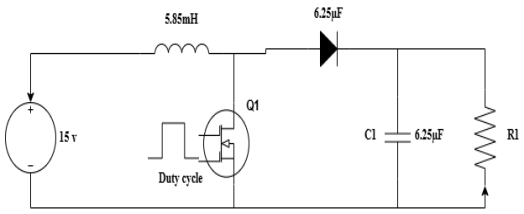

Fig. II.12 *Circuit diagram of boost converter[10].*

5 Model of Wind Turbine Aerodynamics

The kinetic energy of the wind is transformed into mechanical rotational energy for the turbine blades by the wind turbine. The mechanical power P_t generated by the wind turbine is given by :

$$P_t = \frac{1}{2}\rho A C_p(\lambda,\ \beta) v_W^3 \tag{II.43}$$

where $A = \pi R^2$ is the area swept by the rotor blades, R is the radius of the turbine blades, ρ is the air density, λ is the tip speed ratio, β is the blade pitch angle, v_W is the wind speed, and C_p is the power coefficient of the wind turbine.

The tip speed ratio λ is defined as :

$$\lambda = \frac{\omega_m R}{v_W} \tag{II.44}$$

where ω_m is the mechanical angular speed of the turbine rotor.

The power coefficient C_p depends non-linearly on λ and β. According to the literature [37], it can be estimated using the following equations :

$$C_p(\lambda,\ \beta) = c_1 \left(\frac{c_2}{\lambda_i} - c_3\beta - c_4\right) \exp\left(-\frac{c_5}{\lambda_i}\right) + c_6\lambda \tag{II.45}$$

$$\lambda_i = \left(\frac{1}{\lambda + 0.08\beta} - \frac{0.035}{\beta^3 + 1}\right)^{-1} \tag{II.46}$$

which implies :

$$\frac{1}{\lambda_i} = \frac{1}{\lambda + 0.08\beta} - \frac{0.035}{\beta^3 + 1} \tag{II.47}$$

The constants used are : $c_1 = 0.5176$, $c_2 = 116$, $c_3 = 0.4$, $c_4 = 5$, $c_5 = 21$, $c_6 = 0.0068$.

The aerodynamic torque (equal to mechanical torque due to absence of gearbox) is given by :

$$T_w = T_{\text{mec}} = \frac{1}{2}\frac{C_p \rho A R v_W^2}{\lambda} \tag{II.48}$$

It is important to note that the mechanical torque transmitted to the generator is equal to the aerodynamic torque in systems without a gearbox.

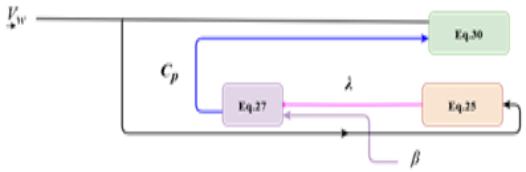

Fig. II.13 *Bloc diagram of wind turbine.*

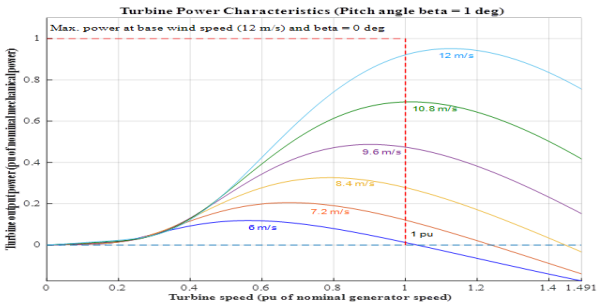

Fig. II.14 *Turbine power characteristics.*

shows the variation of wind power output as a function of wind speed and rotation speed.

6 Permanent magnet synchronous generator :

The turbine weight of this generator can be decreased by doing away with the gearbox. Furthermore, since there are no field windings, there are no rotor losses. In addition, this generator has a high power-to-mass ratio and a very high torque. However, its cost is somewhat exorbitant, and the machine's heating

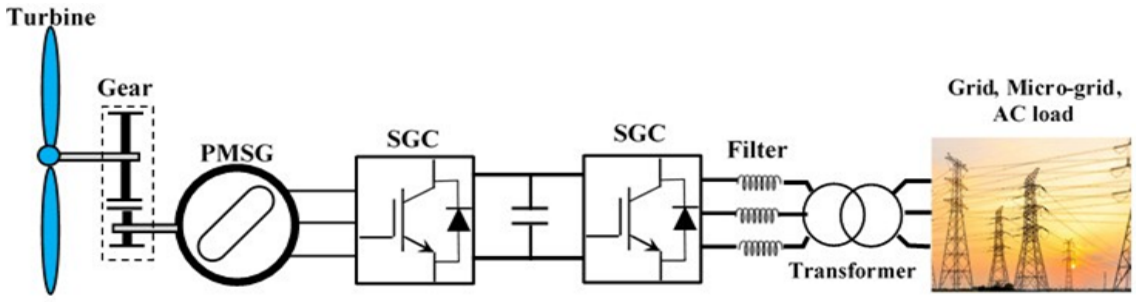

Fig. II.15 *Topology based on synchronous generator with two converters [11].*

The currents I_d and I_q in the Park reference frame have opposite directions for the permanent magnet synchronous generator (PMSG). As a result, the PMSG model can be expressed as :

$$\begin{cases} v_d = -R_s I_d - L_d \dfrac{dI_d}{dt} + \omega L_q I_q \\ v_q = -R_s I_q - L_q \dfrac{dI_q}{dt} - \omega L_d I_d + \omega \phi_f \end{cases} \tag{II.49}$$

Since the stator currents in this operating mode are zero (i.e., $I_d = I_q = 0$), the voltage and torque expressions simplify as follows [38] :

$$\begin{cases} v_d = 0 \\ v_q = \omega \phi_f \\ C_{em} = 0 \end{cases} \tag{II.50}$$

7 MPPT technique

Perturb & Observe is used in this model to achieve maximum output power (MPPT). The dP/dV positions are shown in figure(II.17) The working voltage of the PV array is disrupted by a slight rise in this manner, and the consequent P, the power change, is tracked.The operational point has somewhat shifted to the MPP if the P is positive.Because there are more voltage disturbances in the same direction, this operating point ought to be closest to the MPP. This operating point has shifted away from MPP if P is negative; to get it back to MPP, the perturbation direction should be reversed .The similar technique is applied in wind system technology to attain the highest possible power output .This method is slower.This method is slower than other controllers, such as Fuzzy Logic Con Adaptive FLC (AFLC) and troller (FLC), but we overcame this issue by utilizing low incremental of P&O MPPT . The P&O technique flowchart is displayed in figure(II.18).

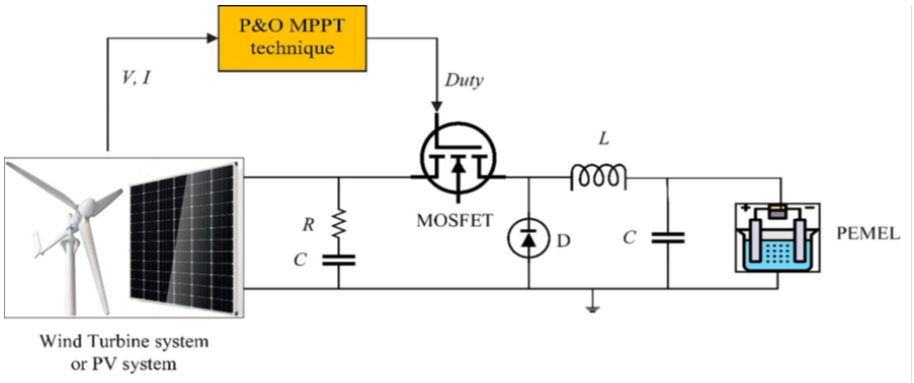

Fig. II.16 *The diagram of the DC-DCbuckconverter.*

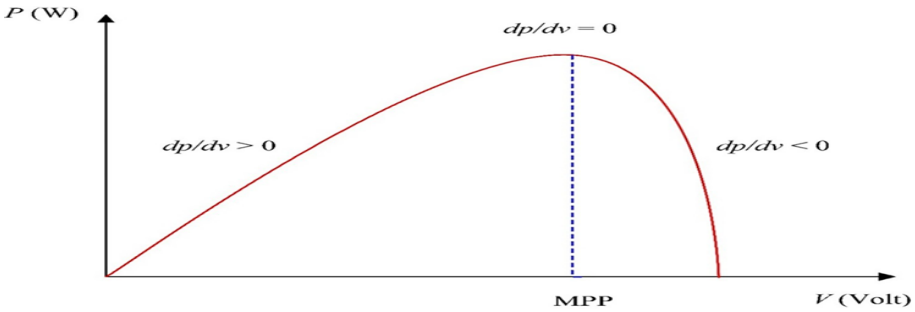

Fig. II.17 *Curve at various points along with the power characteristic P-V.*

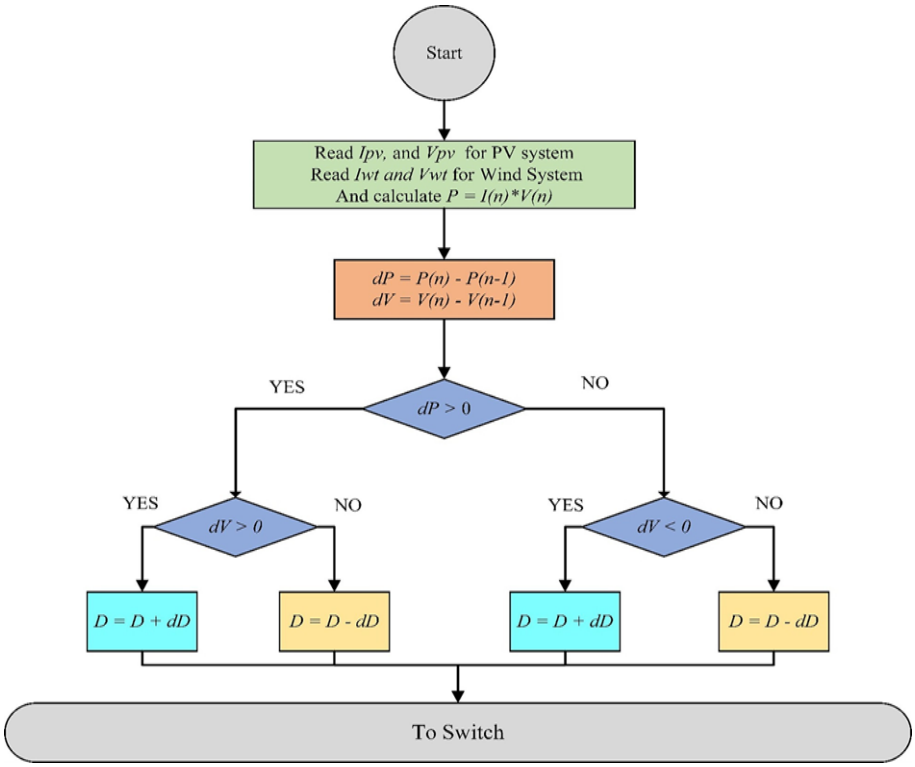

Fig. II.18 *Flowchart of the P&O technique [12].*

8 Design of DC/AC Inverters

DC electric voltage is produced by PV and fuel cells.A power converter is necessary to convert the DC voltage generated by the fuel cell into AC voltage because the majority of industrial and residential loads are AC loads.An AC voltage signal is produced by cutting the DC voltage using IGBT or MOSFET transistors in the power stage of the inverter. Depending on the features and power needed by the load demand, inverters can have single-phase or three-phase voltage. The configuration of the DC/AC inverters in operation is displayed in Figure (II.19). For FC : DC electric voltage is produced by PV and fuel cells. Because the majority of residential and

industrial loads are AC, a power converter is needed to convert the DC

$$P_{\mathrm{DC}} = P_{\mathrm{AC}} \cdot (1 - LF) \tag{II.51}$$

$$I_{\mathrm{DC}} \cdot V_{\mathrm{DC}} = I_{\mathrm{AC}} \cdot V_{\mathrm{AC}} \cdot (1 - LF) \tag{II.52}$$

where V is the voltage (V), I is the current (A), and LF is the loss factor, typically equal to 0.1.

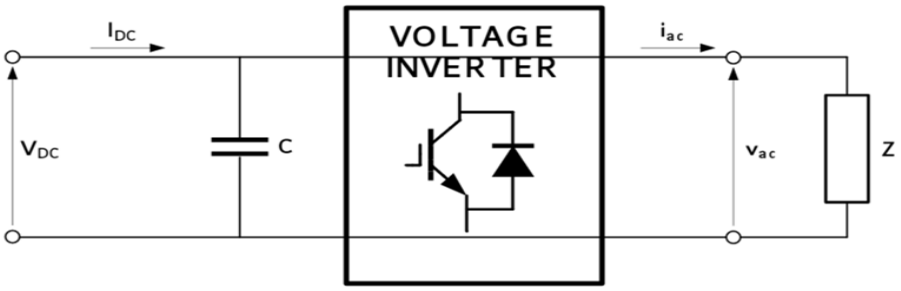

Fig. II.19 *DC/AC inverter design.*

$$I_{\mathrm{DC}} \cdot V_{\mathrm{DC}} = \frac{1}{\sqrt{3}} \cdot P \cdot PF \cdot V_{\mathrm{AC}} \tag{II.53}$$

where PF is the power factor, and it typically ranges from 0.1 to 0.9 [39].

9 Conclusion

This chapter provided a comprehensive overview of green hydrogen production via water electrolysis, with a particular focus on PEM electrolyzers. Among the various electrolyzer types, PEM technology strikes the optimal balance, offering high electrical efficiency, fast response times, and seamless compatibility with renewable energy sources. We explored the fundamental concepts of water electrolysis and the key electrochemical reactions specific to PEM systems. Furthermore, we emphasized that efficient modeling of PV generation systems is critical to facilitate distribution and transfer of renewable energy. A mathematical model was written to simulate the performance of the PV cell, taking into consideration the solar irradiation, temperature, and diode effects. In addition, we also modeled wind turbines and Permanent Magnet Synchronous Generators (PMSGs). Finally,When combined, these detailed models provide a powerful tool for the simulation and optimization of integrated renewable-hydrogen systems. This foundational understanding is essential for formulating efficient and robust green

hydrogen technologies. In the next chapter, we will present and discuss simulation results for a PEM electrolyzer powered by both a direct constant voltage and a hybrid renewable energy source, demonstrating the practical application of these models.

Chapter III

Simulation results of a PEM electrolyzer powered by direct constant voltage and a hybrid source

1 Introduction

In this chapter, we present the control and simulation of the hydrogen production system integrated into a hybrid renewable energy conversion chain. The modeling of the individual system components, such as the electrolyzer, photovoltaic panels, wind turbine, fuel cell, and power converter, has been detailed in Chapter 2. Building upon these models, this chapter focuses on the dynamic simulation of the system under various operating scenarios using MATLAB/Simulink.

The first part of the chapter investigates the behavior of a PEM electrolyzer supplied by a constant voltage source, mimicking the output characteristics of a fuel cell system. This configuration is used to assess the electrolyzer's performance and hydrogen generation efficiency under ideal electrical supply conditions.

The second part extends the study to a more realistic and complex setup in which the electrolyzer is integrated into a hybrid renewable energy system composed of solar and wind energy sources, connected to the electrical grid via a power electronic converter. The simulation evaluates the system's ability to produce hydrogen under variable power inputs and highlights the role of power electronics in ensuring grid compliance and energy stability. A central element of this chapter is the implementation of a Power Management System (PMS), responsible for coordinating energy flows within the hybrid system. The PMS ensures optimal energy distribution, prioritizes renewable energy usage for hydrogen production, and handles energy exchanges with the grid and storage components where applicable.

Moreover, we address the control strategies applied to the key subsystems of the conversion chain, including the renewable generators, the electrolyzer, and the power converter. These control mechanisms are essential for maintaining operational stability, maximizing system efficiency, and adapting to the intermittent nature of renewable energy sources. This simulation study provides a comprehensive assessment of the hydrogen production system's integration into a modern energy architecture, supporting the transition to clean, flexible, and intelligent energy networks.

2 Simulation of the electrolyzer for hydrogen production

In this section, we present the simulation studies carried out using MATLAB/Simulink to evaluate the behavior of an electrolyzer used for hydrogen production under different operating conditions. Two simulation scenarios are considered. In the first scenario, the electrolyzer is powered by a constant voltage source to emulate the output of a fuel cell system. This setup allows for the analysis of the electrolyzer's dynamic response, efficiency, and hydrogen production rate under ideal and controlled voltage supply conditions. The model includes the electrochemical reactions, thermodynamic behavior, and the Faraday efficiency of the electrolyzer, allowing for an accurate representation of hydrogen generation as a function of electrical input. In the second scenario, the electrolyzer is integrated into a hybrid renewable energy conversion chain, which combines sources such as photovoltaic and wind energy. The hybrid system is connected to the power grid via a power electronic converter. This configuration enables the study of real-world operating conditions where input power is variable and influenced by environmental factors. The simulation focuses on the interaction between the fluctuating renewable sources and the electrolyzer, grid integration through the converter, and the overall efficiency of hydrogen production in a smart grid context. Through these simulations, we aim to validate the performance and feasibility of using electrolyzers for green hydrogen production in both standalone and grid-connected renewable energy systems.

3 Simulation results of electrolyzer powered by a constant voltage source

A steady voltage source powers the electrolyzer, simulating a fuel cell system's output. With this configuration, the dynamic response, efficiency, and rate of hydrogen production of the electrolyzer may be analyzed under optimal and regulated voltage supply conditions. Hydrogen creation as a function of electrical input can be accurately represented by the model, which incorporates thermodynamic behavior, electrochemical reactions, and the electrolyzer's Faraday efficiency. and this is the outcome in fugure (III.1) :

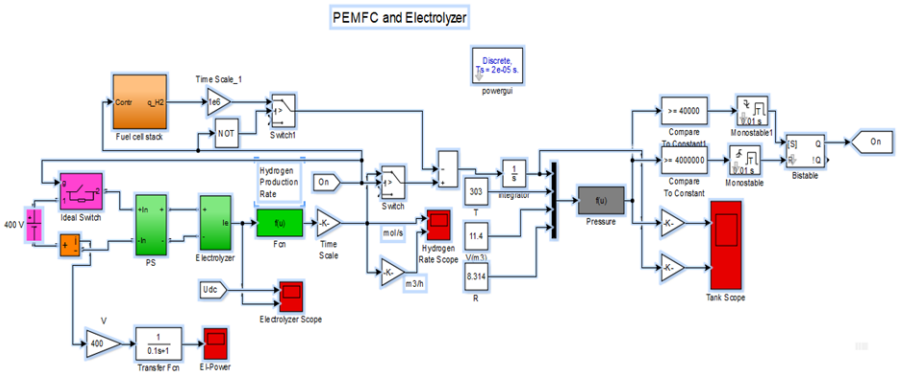

Fig. III.1 *PEMFC and Electrolyzer in MATLAB / Simulink.*

This Simulink model, titled "PEMFC and Electrolyzer," illustrates a system integrating a Proton Exchange Membrane Fuel Cell (PEMFC) with an electrolyzer. The setup appears to simulate hydrogen production, storage, and consumption to manage power flow. It likely represents a smart grid or hybrid energy system with components for control, measurement, and power conversion. A buck converter in a PEMFC simulation primarily regulates the fuel cell's variable output voltage to a stable, lower DC level. This allows for efficient and this is the outcome in figure (III.2)

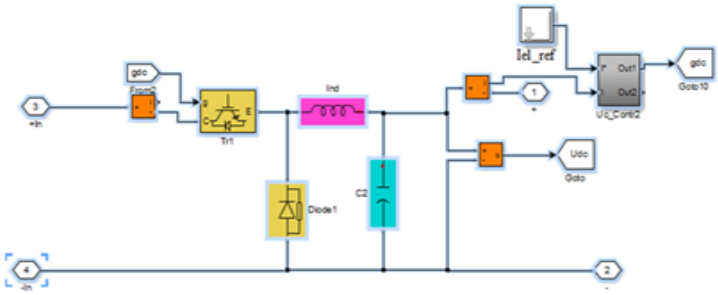

Fig. III.2 *Buck converter in MATLAB / Simulink.*

Figure (III.2) displays a MATLAB/Simulink model of a "Buck converter," as indicated by the caption. The circuit includes a DC voltage source, a switching element (likely a MOSFET or IGBT), an inductor, a capacitor, a diode, and a load. This configuration is typical for a buck converter, which steps down a DC input voltage to a lower DC output voltage.

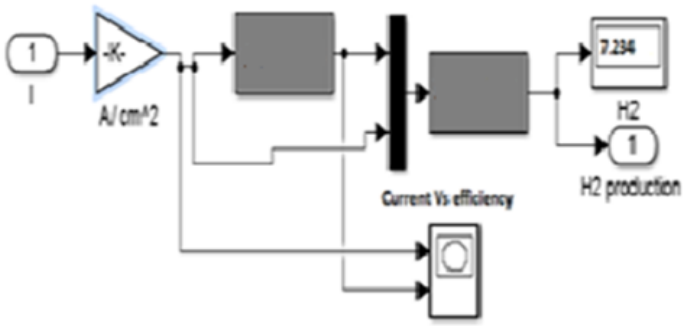

Fig. III.3 *MATLAB/Simulink module for PEM electrolyze.*

This figure (III.3) illustrates the core function of a PEM electrolyzer, showing inputs for current density and outputs for H2 production.

This figure (III.4) titled "MATLAB/Simulink dynamic model for PEM Electrolyzer," depicts a Simulink block diagram. Its role is to visually represent and simulate the dynamic behavior of a Proton Exchange Membrane (PEM) electrolyzer system.

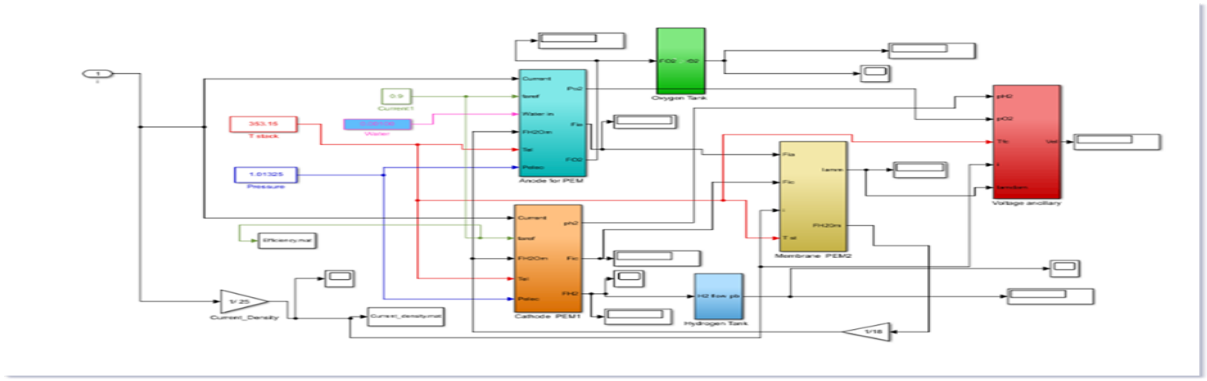

Fig. III.4 *Dynamic response of a PEM electrolyzer system : voltage (a) and current(b) over time.*

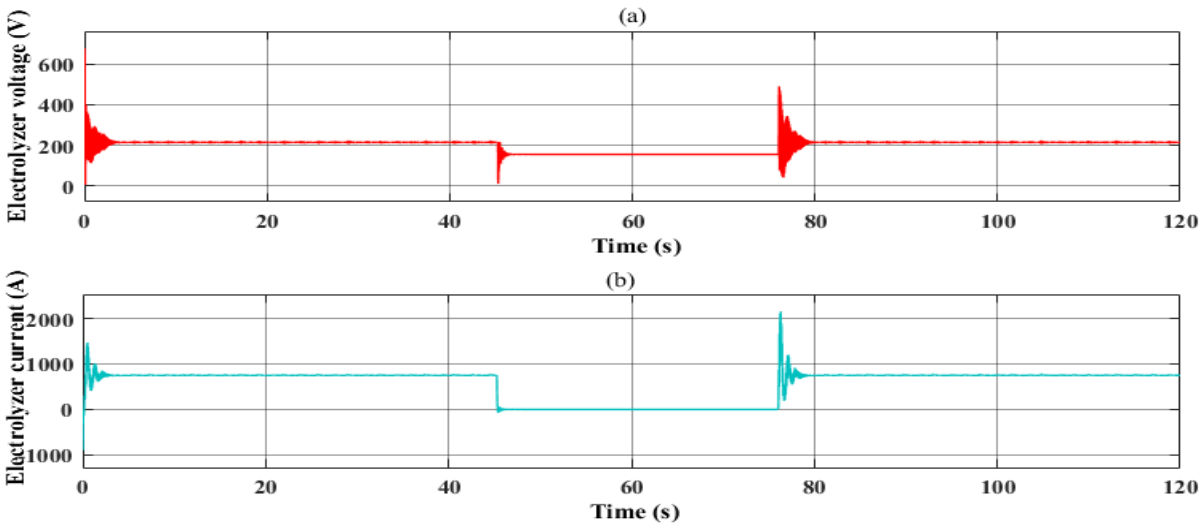

Fig. III.5 *Dynamic response of a PEM electrolyzer system : voltage (a) and current(b) over time.*

Figure (III.5) :At first (III.5.(a)), shows the dynamic response of a PEM electrolyzer system voltage (III.5.(a)) over time. At [0s-40s], the voltage fluctuates and then stabilizes around 200 v. At 43 seconds, the drop to 0 v is caused by a switch from the voltage source to the current from the fuel cell. At 75 seconds, the fluctuation breaks up to 600 v, a cause of fuel cell interaction. The second (III.5.(b)) shows the dynamic response of a PEM electrolyzer system current (III.5.(b)) over time : At [0s-40s], the current is stable around the initial oscillation. At 43 seconds, the current drops to 0 A. At 75 seconds, the current spikes to nearly 2000 A and then stabilizes again around 900 A.

Figure (III.6) : At first (III.6.(a)), shows the dynamic response of a PEM electrolyzer system hydrogen Flow Rate ($mol/s \times 1000$) over time. At [0s-40s], The hydrogen flow rate starts at a high value ($500 mol/s \times 1000$), then gradually decreases with oscillations, settling near zero by 43s. At 43 seconds, the hydrogen flow rate drops sharply to zero is caused by a switch from the voltage source to the current from the fuel cell. At [43s-75s], No hydrogen is produced. At 75 seconds : There is a quick surge in the rate of hydrogen flow, hitting a maximum (almost $1000 mol/s \times 1000$), then resulting in fluctuations before stabilizing close to a consistent rate of about $450 mol/s \times 1000$. This happens at the same time as a significant rise in current to approximately 2000 A, which then levels off around 900 A as referenced in the content.

The second (III.6.(b)) shows the dynamic response of a PEM electrolyzer system hydrogen volume (III.6.(b)) over time : At [0s-43s], oscillates, and gradually drops to zero. At [43s-75s], No hydrogen is produced. At 75 seconds, A sudden increase in the flow rate (nearly

$1.0 \times 10^4 m^3/h \times 1000$) occurred, followed by fluctuations, before it settled at approximately $4.5 \times 10^4 m$ş$/h \times 1000$

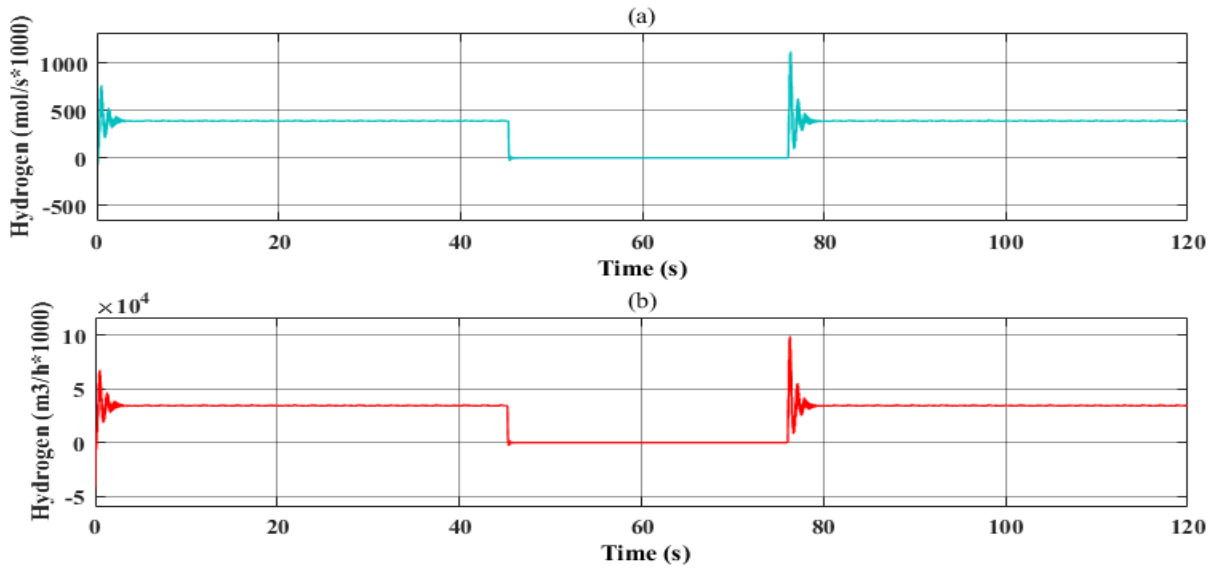

Fig. III.6 *Dynamic response of a PEM electrolyzer system : Hydrogen flow rate (a) , Hydrogen volume (b) over time.*

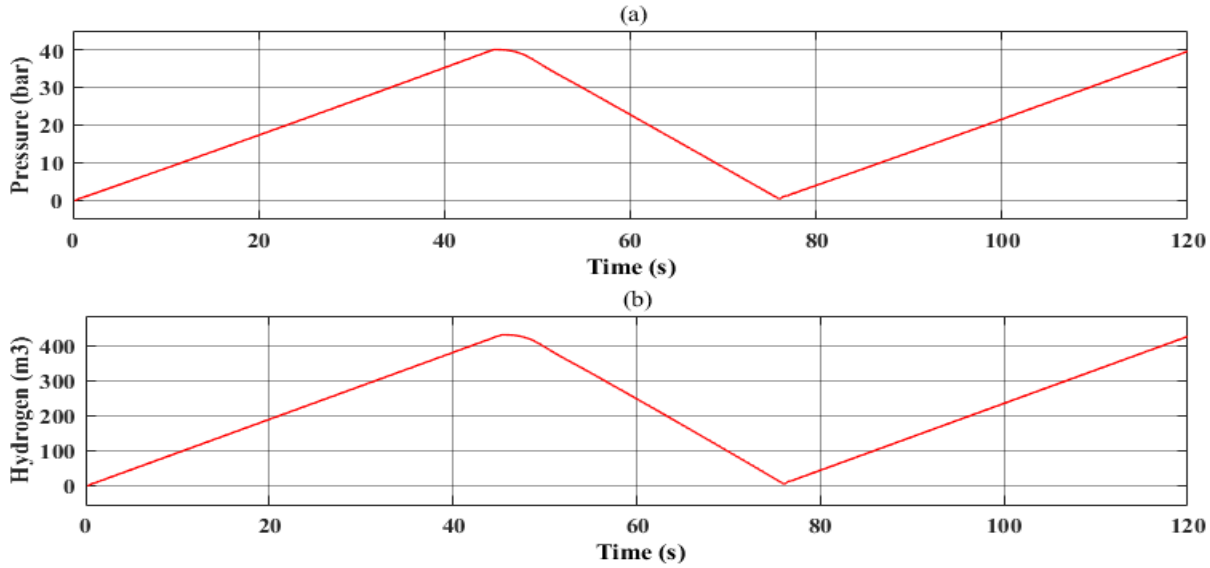

Fig. III.7 *Dynamic response of a PEM electrolyzer system hydrogen volume (a), and (d) Pressure (b) over time.*

Figure (III.7) :At first (III.7.(a))), shows the dynamic response of a PEM electrolyzer system Hydrogen (III.7.(a)) Pressure (bar) over time. At [0s-50s], the pressure increases linearly, reaching a peak around 37 bar. At [50s-75s], the pressure drops rapidly, indicating a release or drop in system pressure. At [75s-120s], The pressure rises once more, but at a comparable speed to the first increase, indicating that the system may be recovering or restarting.

The second (III.7.(b)) shows the dynamic response of a PEM electrolyzer system hydrogen volume (b) over time : At [0s-50s], It rises gradually, reaching around $400cm^3$. At [50s-75s], indicating hydrogen release or system shutdown.At [75s-120s], The volume then rises

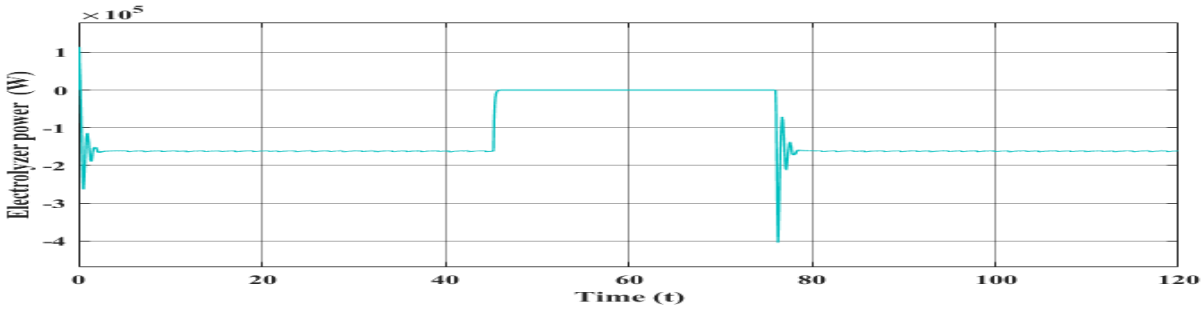

Fig. III.8 *Dynamic response of a PEM electrolyzer system : Power over time.*

Figure (III.8) : shows the dynamic response of a PEM electrolyzer Power (W) over time.At [0s-45s], The power stays approximately the same at $-2Ö10^5W$, which shows consistent energy use by the electrolyzer while producing hydrogen, The negative figure indicates that this power is being consumed rather than produced. At [45s-75s], Power abruptly increases to 0 W. At 75 seconds, A short surge or change happens when the system returns to providing power ; this is a temporary reaction caused by the switching process.

4 Integration of a hybrid renewable energy conversion chain.

This section presents the simulation results and analysis of a multisource energy system for hydrogen production, integrating photovoltaic (PV) panels, a wind turbine, and an electrolyzer. The system is analyzed under varying wind speed profiles and solar irradiation conditions. The results include the key electrical and operational characteristics, such as voltage, current, power, hydrogen flow rate, pressure, and storage dynamics. Additionally, grid characteristics (three-phase voltage and current) and power management among the different subsystems are examined

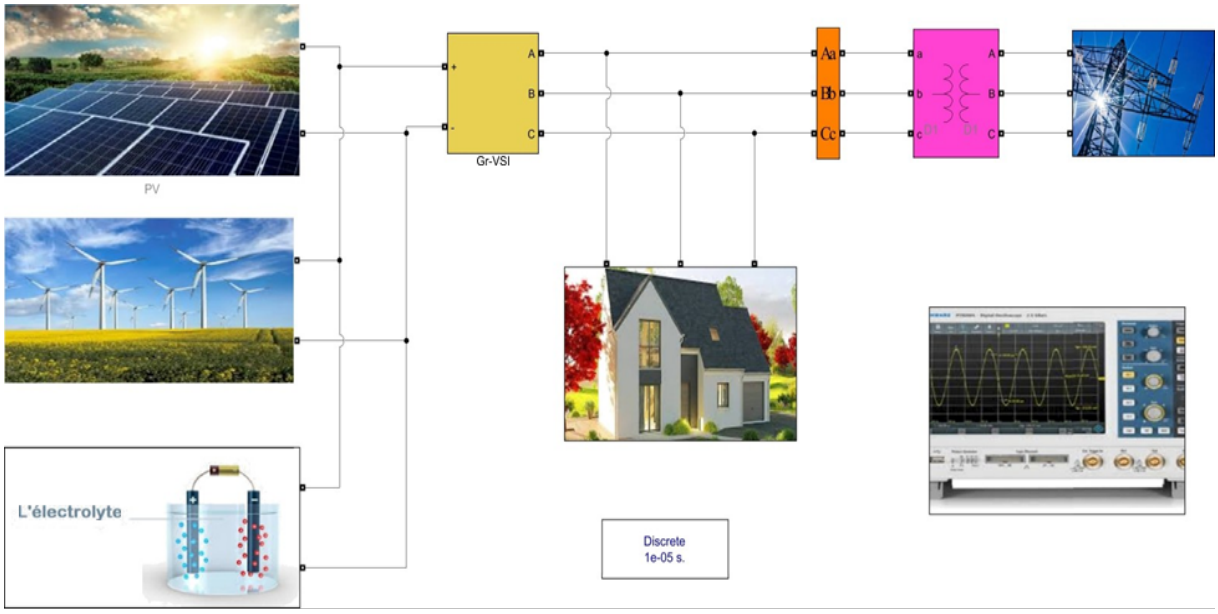

Fig. III.9 *Simulink model for the integration of an electrolyzer into an energy system .*

This figure(III.9), illustrates a Simulink model for the integration of an electrolyzer into an energy system. It shows various energy sources like solar PV and wind turbines connected to an electrolyzer and a residential load, with what appears to be a power grid connection and a scope for viewing simulation results. These elements require rigorous and optimal energy management to achieve good performance in the overall energy balance.

5 Simulation results of electrolyzer integration

The simulation validation was conducted to assess the effectiveness of the global control scheme, and the parameter values utilized are detailed in Table A.1 of the Appendix. To ensure that the output parameters remain within acceptable limits, it is important to implement a suitable regulation mechanism. Accordingly, a proposed solution involves the incorporation of an active front-end DC-AC converter, which can enhance the power quality of the system, making it suitable for grid connection.

6 Voltage, Current, and Power Profiles

The power and current outputs of t wind turbine exhibit fluctuations corresponding to the varying irradiation and wind profiles. Figure (III.10) show the input rotational speed of the generator and the corresponding mechanical torque generated. A negative torque value

indicates that the machine is functioning as a generator. Figure (III.11)also illustrates the output electromagnetic torque produced by the generator.

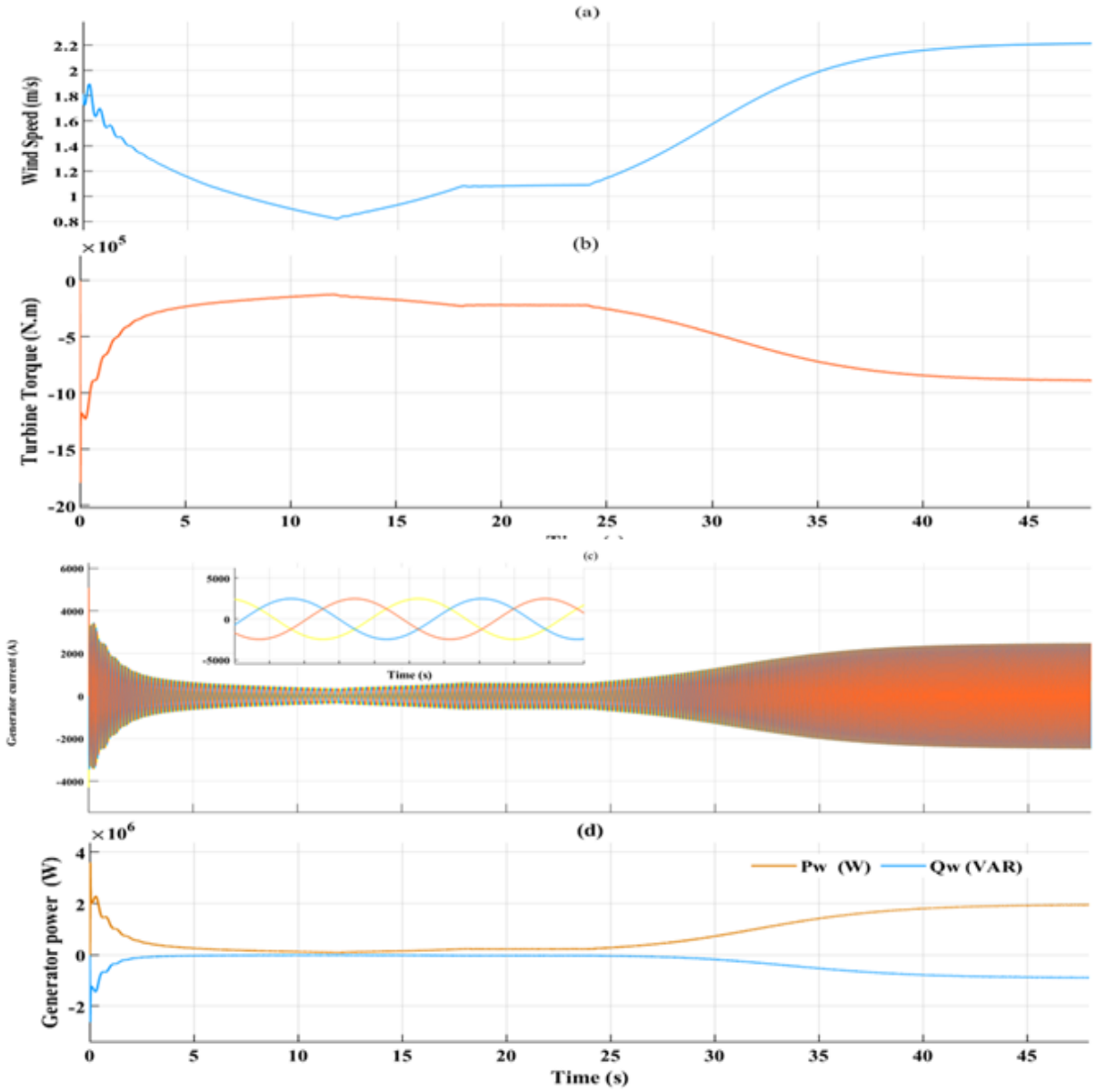

Fig. III.10 *Wind turbine characteristics for hydrogen production – power, torque, and efficiency profiles under varying wind speeds .*

This figure (III.10). Wind turbine characteristics for hydrogen production – power, torque, current and efficiency profiles under varying wind speeds," shows four plots detailing the dynamic response of a wind turbine system. Figure (III.10 (a)) shows the wind speed varying over time. It starts at a relatively high speed, drops to a lower speed around 10-15 seconds, and then gradually increases again. This fluctuating wind speed is the primary input driving the turbine's behavior.

Figure (III.10 (b)) represent the torque produced by the wind turbine. It closely follows the trend of the wind speed. As wind speed decreases, the torque also decreases, and as wind speed increases, the torque rises. This indicates a direct relationship between the available wind energy and the mechanical output of the turbine.

Figure (III.10 (c)) shows the current generated by the wind turbine. It exhibits significant fluctuations, especially during changes in wind speed. Initially, there's a large current peak, which then settles down, but still shows oscillations, particularly when the wind speed is lower. This suggests the generator is actively responding to the varying power input from the turbine.

Figure (III.10 (d)) displays both the active power (Pw, in Watts) and reactive power (Qw, in VAR) generated. The active power largely mirrors the trends of wind speed and torque, indicating the actual power delivered by the system. The reactive power (Qw) also shows a response, which is crucial for grid stability and power factor correction, though its specific behavior would depend on the control strategy implemented.

6.1 Hydrogen Flow Rate, Pressure, and Storage Dynamics

The electrolyzer converts the electrical energy from the PV panels and wind turbine into hydrogen, with its flow rate directly dependent on the power supplied. In Figure (III.11), the hydrogen production rate shows significant variations in response to the changing renewable energy inputs.

This four-panel figure (III.11) illustrates the dynamic response of a PEM electrolyzer system to step changes in current over 48 seconds. Panel (III.11 (a)) shows the applied current, which alternates between periods of positive current (around 300 A) and zero current, driving the electrolyzer. Panel (III.11 (b)) displays the hydrogen flow rate, which directly mirrors the current, showing positive flow (around 700 mol/s) when current is applied and dropping to zero when the current is off, indicating the system's immediate hydrogen production capability. Consequently, Panel (III.11 (c)) demonstrates the hydrogen volume, which steadily increases during periods of hydrogen production and then gradually decreases when production stops (likely due to consumption or venting), resulting in a sawtooth-like profile. Finally, Panel (III.11 (d)) reveals the pressure within the system, which also follows a sawtooth pattern, increasing as hydrogen volume accumulates and decreasing when production ceases, with a peak pressure of approximately 40 bar, indicating the system's ability to store the produced hydrogen under pressure.The pressure inside the hydrogen storage tank increases steadily as the production

progresses, demonstrating the system's capability to store hydrogen effectively. Storage levels are monitored to ensure safe and efficient operation under varying conditions.

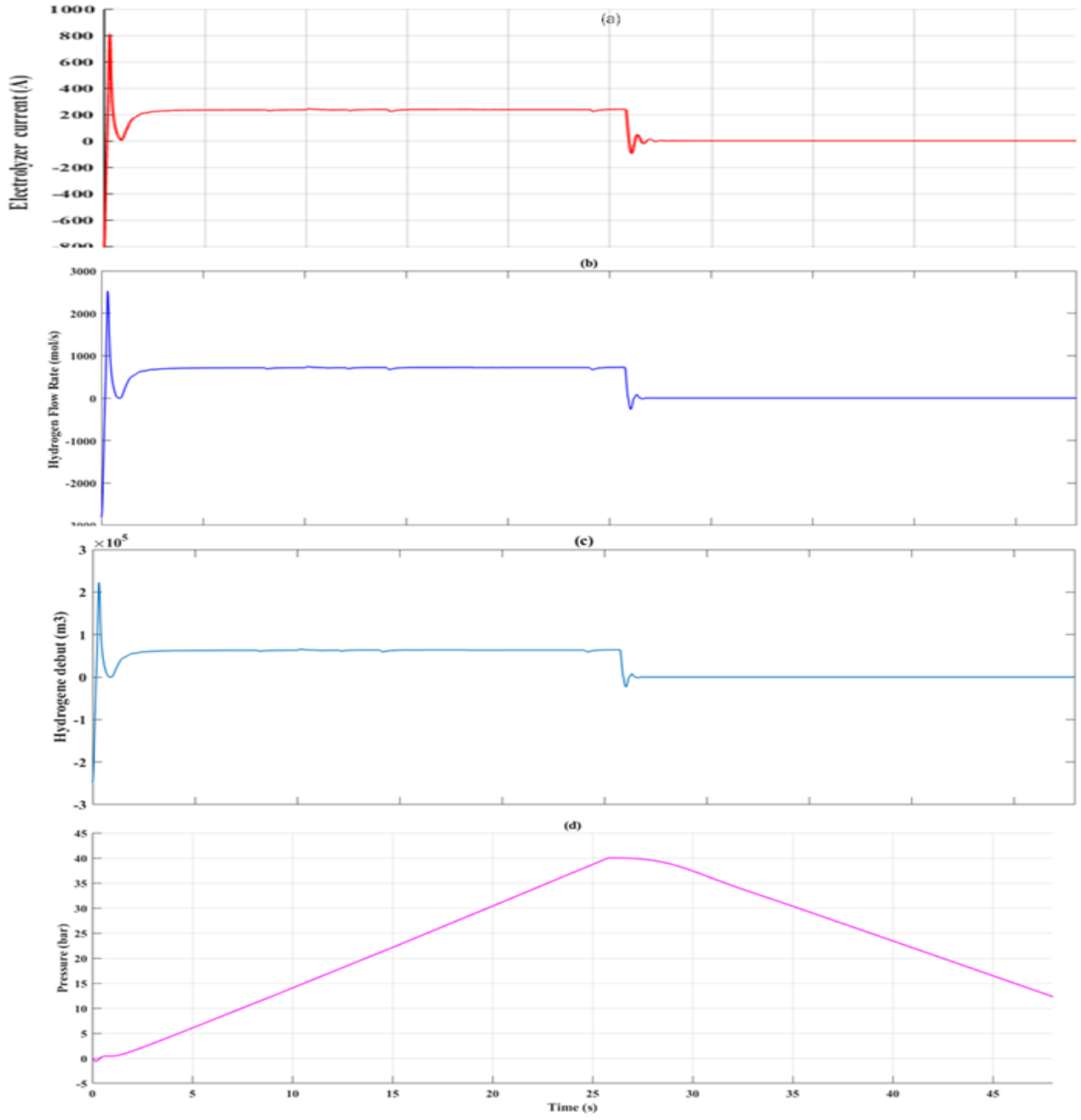

Fig. III.11 *Dynamic response of a PEM electrolyzer system : (a) Current, (b) Hydrogen flow rate, (c) Hydrogen volume, and (d) Pressure over time.*

6.2 Grid Characteristics

The integration of the multisource system with the grid is analyzed through the three-phase voltage and current characteristics. During the process of wind speed fluctuation, there is a decrease in grid voltages which can be addressed by implementing a control strategy that can improve the voltage level. Additionally, the use of a compensator can also eliminate the issue of

voltage sagging. The stability of the DC voltage is maintained, as evidenced by Figure (III.13), which demonstrate that both the AC current and voltage delivered are sinusoidal in nature. The grid voltage remains stable around 500 V, while the current reflects the power flow dynamics, accommodating the varying contributions from the renewable sources and load demands. The control system ensures seamless interaction between the (III.12)III.12. These findings indicate the effectiveness of the control strategy implemented in the converter, resulting in higher quality energy output.

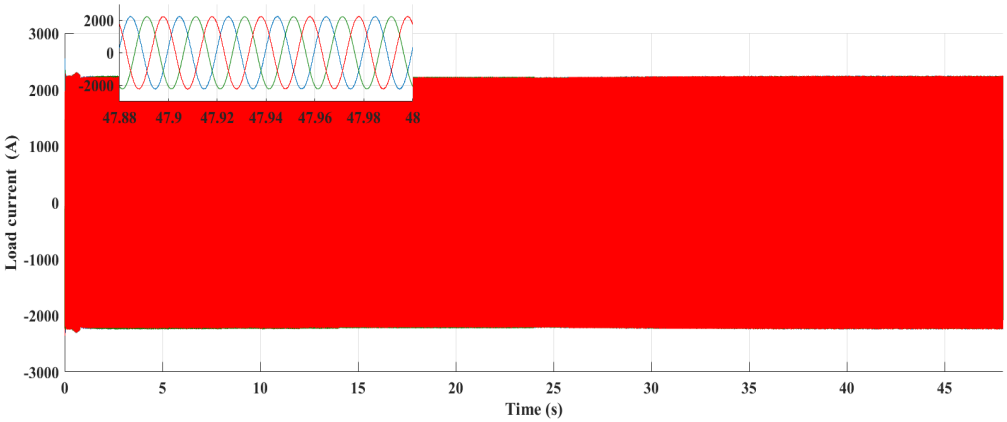

Fig. III.12 *Performance analysis of load : (a) Three-phase stator currents, (b) Three-phase rotor currents and its zoom.*

The first figure (III.12). presents a one-panel view of a three-phase load, displaying its current characteristics over 48 seconds. illustrates the load current, which also exhibits a stable three-phase behavior, with its inset showing sinusoidal waveforms peaking at around 2000 A, indicating a consistent power draw by the load. The simulation results demonstrate that the DC bus voltage remains stable throughout the operation of the multisource energy system. Despite the variability in wind speed and solar irradiation, the DC bus voltage experiences only small fluctuations over time. These variations are limited to approximately 5% of the nominal voltage, indicating effective regulation by the power converters and control system. Figure III.13 shows the DC voltage at each level of the converter, demonstrating that the DC voltage at each level stays close to its reference value, with only slight fluctuations during transient periods.

Figure (III.13) shows the DC voltage at each level of the converter, demonstrating that the DC voltage at each level stays close to its reference value, with only slight fluctuations during transient periods.

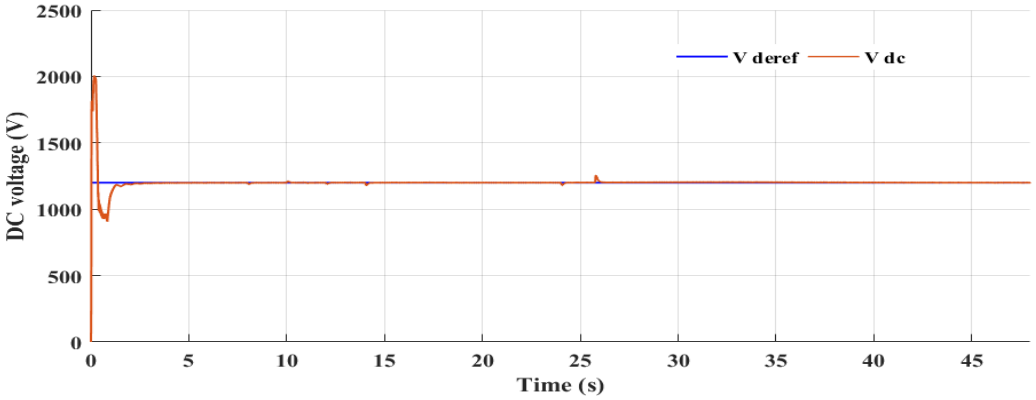

Fig. III.13 *Regulated DC bus voltage.*

This figure (III.13) illustrates the performance of a DC bus voltage regulation system over a 48 second period. The red line represents the reference DC voltage ($V_{\mathrm{dc,ref}}$), which is set to a constant value of approximately 1200 V. The blue line, representing the actual DC voltage (V_{dc}), closely tracks this reference, indicating successful voltage regulation. Despite some initial transient spikes (around 0-5 seconds) and noticeable dips at approximately 45 second, as well as smaller upward spikes around 28 seconds, the system consistently returns the DC bus voltage to the desired 1200 V, demonstrating robust control and effective rejection of disturbances.

The observed stability ensures reliable energy delivery to the electrolyzer and other connected components. Minor transient deviations occur during sudden changes in renewable energy inputs, but the control system rapidly restores the voltage to its nominal value. This highlights the robustness of the DC bus voltage regulation, which is essential for maintaining system efficiency and protecting critical components in the hydrogen production process.

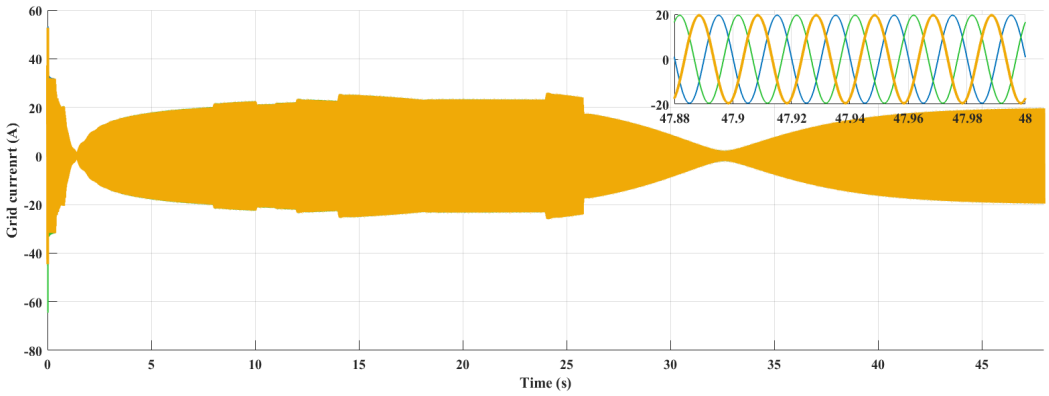

Fig. III.14 *Characteristics of the power grid : (a) Voltage, (b) Current grid and its zoom.*

Thi figure (III.14) illustrates the stability of the grid current .

This figure (III.14) illustrates the stability of the grid voltage and the dynamic behavior of the grid current in a three-phase power system over 40 seconds. depicts the grid current, exhibits significant fluctuations between approximately -40 A and 20 A, suggesting varying power exchange with a connected system ; its inset also reveals sinusoidal three-phase waveforms at around $20A$ amplitude during a period of dynamic activity, confirming the alternating current nature despite the overall variability. the grid voltage, which maintains a stable base level around $5000V$ over all.

6.3 Energy management in hybrid PV/wind electrolysis systems

Power management in green hydrogen production using wind and photovoltaic (PV) systems, along with electrolyzers, aims to optimize the real-time utilization of renewable energy sources. As illustrated in Figure III.15, the wind and PV systems are connected to the electrical grid and supply the electricity required to operate the electrolyzer for hydrogen generation.

The electrolyzer uses the available renewable energy to split water into hydrogen and oxygen. The power management system ensures that the electrolyzer operates efficiently by adjusting its performance according to grid demand and renewable energy supply. This approach maximizes the use of clean energy for hydrogen production while maintaining grid stability and supporting a low-carbon economy.

The power management system dynamically distributes the energy produced by the PV panels, wind turbine, and the grid. The power generated by each source as shown in figure (III.16) is directed to meet the load demand and power the electrolyzer for hydrogen production. The results illustrate the effective coordination of power flows, ensuring balanced operation even under varying environmental conditions. The contributions of wind and PV power are prioritized, with grid power serving as a supplementary source to maintain system stability and maximize renewable energy utilization.

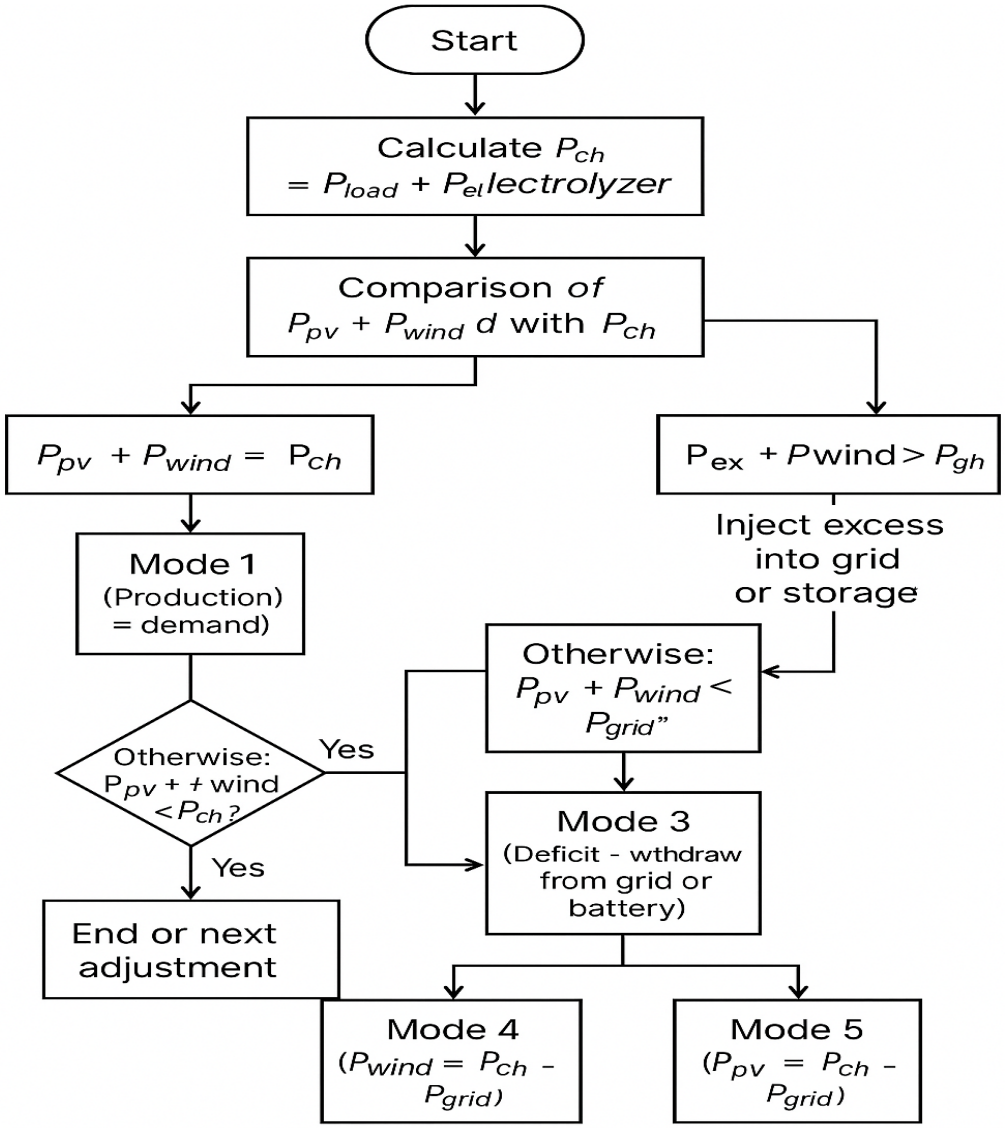

Fig. III.15 *Power Management flowchart for off-grid Green hydrogen production with a hybrid PV/wind-to-electrolysis system.*

The simulation study demonstrates that the power generation system implemented in this study intelligently determines the appropriate combination of energy conversion chain based on hybrid sources to respond to the integration of the energy produced in the power grid while maintaining satisfactory connection conditions of the electrolyser for hydrogen production process. Nevertheless, it is essential to ensure that the energy delivered to the grid is of high quality, characterized by harmonics-free voltage and current waveforms, and a regulated DC bus voltage. To achieve this, the effectiveness of using a voltage source inverter controlled by the advanced control strategy is evaluated in the obtained results.

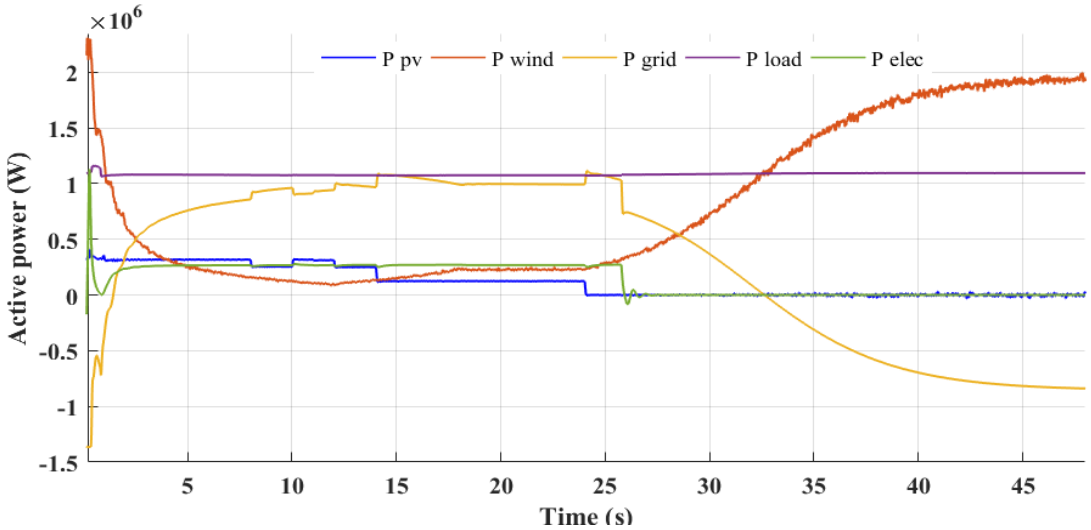

Fig. III.16 *Power Management overview – wind power, PV power, grid power, load power, and electrolyzer power distribution.*

These results demonstrates that both the grid voltage and the DC link voltage are regulated even under fluctuating generator speeds and irradiation change. To ensure a power factor of unity, the stator's active power injected into the grid is regulated using the MPPT strategy, while the reactive power is held at zero. The obtained simulation results provide insight into the effectiveness of control strategies to maximize output power, regulate active and reactive power, and ensure a stable connection to the grid. These results show that the MPPT control strategy can track the maximum power point of the Wind-PMSG system under various wind conditions, resulting in maximum power output. Likewise, active power control and reactive power control can maintain a stable and reliable connection to the grid while regulating the system output power.

7 Conclusions

In this chapter, we have carried out a comprehensive simulation study of a hydrogen production system based on a proton exchange membrane electrolyzer using MATLAB/Simulink. Starting from the individual modeling of components established in Chapter 2, we simulated two main configurations : an electrolyzer powered by a constant voltage source representing an ideal fuel cell, and a more realistic scenario where the electrolyzer is integrated into a hybrid renewable energy system composed of photovoltaic and wind energy sources.

The simulation results confirmed the dynamic behavior and efficiency of the electrolyzer

under both steady and variable power conditions. The second configuration, involving the integration of renewable sources and a power converter connected to the grid, demonstrated the system's feasibility for real-world applications. Special attention was given to the design and implementation of a Power Management System, which ensures optimal coordination between generation, storage, hydrogen production, and grid interaction. Furthermore, the chapter highlighted the importance of control strategies in maintaining the performance, stability, and reliability of each subsystem within the conversion chain. The applied control schemes enabled efficient regulation of power flows and contributed to maximizing the utilization of renewable resources for green hydrogen production.

This simulation study forms the basis for further analysis and optimization, particularly in relation to real-time control implementation, energy cost analysis, and the integration of storage solutions for enhancing system autonomy and flexibility.

General conclusion

General conclusion

General conclusionl

This study comprehensively investigates the potential for off-grid green hydrogen production in the Algerian Sahara, highlighting its critical role in fostering sustainable energy solutions. By harnessing the abundant renewable energy resources of the region through a hybrid photovoltaic-wind system, the research demonstrates a viable pathway for decentralized hydrogen generation. The detailed modeling of system components, including electrolyzers and renewable energy profiles, provides a robust framework for understanding system performance. Crucially, the simulation results validate the effectiveness of powering a PEM electrolyzer directly with a constant voltage and through a hybrid source, underscoring the technical feasibility and efficiency of the proposed off-grid approach. The Algerian Sahara, with its exceptional solar and wind potential, emerges as an ideal location for such initiatives, offering a promising avenue for decarbonization, energy independence, and the development of a green hydrogen economy.

Chapter 1 deals with The Algerian Sahara possesses immense and largely untapped renewable energy potential, particularly solar and wind resources.1 This chapter concludes that the high solar irradiance and consistent wind speeds prevalent across the region make it an exceptionally favorable location for large-scale renewable energy projects. Quantitative analysis of these resources confirms their sufficiency to power energy-intensive processes like green hydrogen production. The geographical advantages of the Sahara, coupled with the imperative for sustainable development, position it as a strategic hub for renewable energy generation, offering a clean and virtually inexhaustible energy supply for various applications, including hydrogen production.

This chapter concludes that accurate and comprehensive modeling of system components, specifically the electrolyzer and the profiles of renewable energy sources (photovoltaic and wind), is paramount for the effective design and simulation of off-grid green hydrogen production

systems. The developed models successfully capture the dynamic behavior and characteristics of PEM electrolyzers under varying operating conditions, as well as the fluctuating nature of solar and wind power generation.2 This detailed modeling provides a crucial foundation for understanding the interdependencies between energy supply and hydrogen production, enabling precise system sizing, optimization, and the identification of potential operational challenges and solutions for ensuring stable and efficient hydrogen output.

Bibliographie

[1] Youcef Himri, Shafiqur Rehman, Ali Mostafaeipour, Saliha Himri, Adel Mellit, Mustapha Merzouk, and Nachida Kasbadji Merzouk. Overview of the role of energy resources in algeria's energy transition. *Energies*, 15(13) :4731, 2022.

[2] Younes Zahraoui, Mohammed Reyasudin Basir Khan, Ibrahim Alhamrouni, et al. Current status, scenario, and prospective of renewable energy in algeria : a review. *Energies*, 14(9) :2354, 2021.

[3] Soumia Rahmouni, Belkhir Negrou, Noureddine Settou, et al. Prospects of hydrogen production potential from renewable resources in algeria. *International Journal of Hydrogen Energy*, 42(2) :1383–1395, 2017.

[4] Michel Noussan, Pier Paolo Raimondi, Rossana Scita, and Manfred Hafner. The role of green and blue hydrogen in the energy transition—a technological and geopolitical perspective. *Sustainability*, 13(1) :298, 2020.

[5] Asma Chabani, Salim Makhloufi, and Salah Lachtar. Overview and impact of the renewable energy plants connected to the electrical network in southwest algeria. *EAI Endorsed Transactions on Energy Web*, 8(36) :e7–e7, 2021.

[6] Negin Behesht Nejad. Optimization of hydrogen production planning through electrolysis, 2021. Pages 757.

[7] Radenka Maric and Haoran Yu. Proton exchange membrane water electrolysis as a promising technology for hydrogen production and energy storage. In *Nanostructures in Energy Generation, Transmission and Storage*, page 13. 2019.

[8] Javier Vinuelas Ferrando. *Modelling and Simulation of Hydrogen Electrolyzers for Power System Applications*. PhD thesis, Unknown Institution, 2023. Thèse, informations détaillées à compléter.

[9] B. Djerad, X. Zhang, J. Smith, et al. Characterisation of a pem electrolyser using the current interrupt method. *International Journal of Hydrogen Energy*, 2016. Modèles 3 et 4 sans surpotentiel de la cathode, avec impédance Randles–Warburg.

[10] Sivasankar Nallusamy and D. Kaliaperumal Rukmani. Design and simulation of arduino nano controlled dc-dc converters for low and medium power applications. *International Journal of Electrical and Computer Engineering (IJECE)*, 13(2) :1400–1408, 2023.

[11] Larbi Chrifi-Alaoui, Saïd Drid, Mohammed Ouriagli, et al. Overview of photovoltaic and wind electrical power hybrid systems. *Energies*, 16(12) :4778, 2023.

[12] Mohamed Awad, Mohamed Metwally Mahmoud, Z. M. S. Elbarbary, et al. Design and analysis of photovoltaic/wind operations at mppt for hydrogen production using a pem electrolyzer : Towards innovations in green technology. *PLOS ONE*, 18(7) :e0287772, 2023.

[13] Khaled Hasan, Sumaiya Binty Yousuf, Mohammad Shahed Hasan Khan Tushar, et al. Effects of different environmental and operational factors on the pv performance : A comprehensive review. *Energy Science and Engineering*, **10**(2) :656–675, 2022.

[14] M. Jayachandran, Ranjith Kumar Gatla, Aymen Flah, et al. Challenges and opportunities in green hydrogen adoption for decarbonizing hard-to-abate industries : A comprehensive review. *IEEE Access*, 12 :23363–23388, 2024.

[15] Swetha Bhagwat and Maria Olczak. Green hydrogen : bridging the energy transition in africa and europe. Technical report, European University Institute, 2020.

[16] Peter Schossig, Peter Droege, Antonia Riemer, and Martin Speer. *Proceedings of the International Renewable Energy Storage Conference (IRES 2022)*, volume 16. Springer Nature, 2023.

[17] A. A. Kazem and M. T. Chaichan. Dust effect on photovoltaic utilization in iraq : Review article. *Renewable and Sustainable Energy Reviews*, 37 :734–749, 2014.

[18] B. Guo, Z. Liu, Y. Lv, and Y. Wang. Effect of dust on the performances of pv modules in a desert region. *Energy Procedia*, 75 :307–312, 2015.

[19] B. M. Usov. Dust storms in central asia : Causes and consequences. *Meteorology and Hydrology*, 5 :24–30, 1991.

[20] F. Touati, M. Benhaddadi, and A. Massoud. Impact of environmental factors on pv system performance in qatar. *Renewable Energy*, 113 :1451–1466, 2017.

[21] N. Jones, M. Harrison, and K. Lawrence. Seasonal variations of dust and its effects on solar panel efficiency. *Environmental Science and Technology*, **52**(12) :7077–7085, 2018.

[22] S. Nižetić, D. Čoko, A. Yadav, and F. Grubišić-Čabo. Photovoltaic panels : A review of cooling techniques. *Renewable and Sustainable Energy Reviews*, 67 :1340–1358, 2017.

[23] S. Nižetić, A. Yadav, and F. Grubišić-Čabo. Experimental investigation of passive and active cooling of pv panels. *Energy*, 139 :1173–1184, 2018.

[24] K. Badi, M. Mekhilef, and A. Saidur. Dust deposition impact on photovoltaic performance : A review. *Solar Energy*, 160 :145–159, 2018.

[25] S. Ghazi, K. Sayigh, and A. Rehman. Dust effect on flat surfaces : A review. *Energy Reports*, 1 :12–22, 2014.

[26] Arturo Vallejos-Romero, Minerva Cordoves-Sánchez, César Cisternas, et al. Green hydrogen and social sciences : issues, problems, and future challenges. *Sustainability*, 15(1) :303, 2022.

[27] Jayant Sinha. Innovations and challenges of green hydrogen applications in energy transition, 2022. Senior Principal Consultant.

[28] Shannon W. Boettcher. Introduction to green hydrogen. *Chemical Reviews*, 124(23) :13095–13098, 2024.

[29] Joonas Koponen, Antti Kosonen, Kimmo Huoman, et al. Specific energy consumption of pem water electrolysers in atmospheric and pressurised conditions. In *2016 18th European Conference on Power Electronics and Applications (EPE'16 ECCE Europe)*, pages 1–10. IEEE, 2016.

[30] Samir Touili, Ahmed Alami Merrouni, Youssef El Hassouani, et al. Analysis of the yield and production cost of large-scale electrolytic hydrogen from different solar technologies and under several moroccan climate zones. *International Journal of Hydrogen Energy*, 45(51) :26785–26799, 2020.

[31] ARARIA Rabah. *Contribution à la Modélisation et la Commande d'un Véhicule Electrique Hybride à Architecture Série/Parallèle (Étude Théorique et Expérimentale)*. PhD thesis, Université Ibn Khaldoun-Tiaret-, 2020.

[32] Mahyar Tofighi-Milani, Sajjad Fattaheian-Dehkordi, and Matti Lehtonen. Electrolysers : a review on trends, electrical modeling, and their dynamic responses. *IEEE Access*, 2025.

[33] Z. Aouali, A. Mellit, H. Mekki, and M. Bouzguenda. Modeling and simulation of a photovoltaic module in matlab/simulink environment. *International Journal of Electrical and Computer Engineering (IJECE)*, 4(6) :872–880, 2014.

[34] S. Dey, A. K. Roy, and S. Bandyopadhyay. Mathematical modeling and simulation of photovoltaic cell using matlab/simulink environment. *International Journal of Emerging Technology and Advanced Engineering*, 6(3) :90–97, 2016.

[35] S. S. Chandel, M. Nagaraju, and A. Agarwal. Modeling and performance analysis of a solar photovoltaic cell using matlab/simulink. *Materials Today : Proceedings*, 18 :3030–3036, 2019.

[36] S. Sheik Mohammed and D. Devaraj. Design, simulation and analysis of microcontroller based dc-dc boost converter using proteus design suite. In *Proc. of Int. Conf. on Advances in Electrical & Electronics (AETAEE)*, pages 599–606, 2013.

[37] Piotr Gajewski and Krzysztof Pieńkowski. Control of the hybrid renewable energy system with wind turbine, photovoltaic panels and battery energy storage. *Energies*, 14(6) :1595, 2021.

[38] Fatima Zohra Naama, Abdallah Zegaoui, Yssaad Benyssaad, et al. Model and simulation of a wind turbine and its associated permanent magnet synchronous generator. *Energy Procedia*, 157 :737–745, 2019.

[39] Hussein A. Z. Al-Bonsrulah, Mohammed J. Alshukri, Lama M. Mikhaeel, et al. Design and simulation studies of hybrid power systems based on photovoltaic, wind, electrolyzer, and pem fuel cells. *Energies*, 14(9) :2643, 2021.

ملخص:

تتناول هذه الدراسة جدوى إنتاج الهيدروجين الأخضر في الصحراء الجزائرية، من خلال نظام هجين خارج الشبكة يجمع بين الطاقة الشمسية الكهروضوئية وطاقة الرياح، مدمجًا بعملية التحليل الكهربائي. تمثل وفرة مصادر الطاقة الشمسية والرياح في المنطقة عاملاً محفزًا لإنشاء نموذج إنتاج طاقة مستدامة. يعتمد النظام المقترح على تقنية متقدمة لتحويل التيار المستمر (DC-DC) تهدف إلى تحسين تدفق الطاقة من المصادر المتجددة نحو المحلل الكهربائي، بما يضمن إنتاجًا فعالًا للهيدروجين تحت ظروف بيئية متغيرة .يشمل تحليل الأداء تقييم موثوقية النظام وكفاءة تحويل الطاقة وكميات الهيدروجين المنتجة خلال فصول السنة المختلفة. تظهر النتائج الإمكانات العالية لهذا النموذج الهجين في تقديم حلول طاقة نظيفة ومتجددة لإنتاج الهيدروجين، مما يُسهم في تقليل الاعتماد على الوقود الأحفوري ومواجهة تحديات الطاقة العالمية. ويُبرز هذا العمل أهمية دمج أنظمة الطاقة المتجددة في المناطق النائية لدعم التنمية المستدامة وتعزيز استراتيجيات الانتقال الطاقوي.

الكلمات المفتاحية: الهيدروجين الأخضر، النظام الهجين للطاقة الشمسية والرياح، محولDC-DC ، الطاقة خارج الشبكة، التحليل الكهربائي.

Résumé

This study investigates the feasibility of green hydrogen production in the Algerian desert through an off-grid hybrid energy system combining photovoltaic solar and wind power, integrated with an electrolysis process. The region's abundant solar and wind resources make it an ideal location for sustainable energy production. The proposed system employs advanced DC-DC conversion technology to optimize energy flow from renewable sources to the electrolyzer, thereby ensuring efficient hydrogen production under varying environmental conditions. The performance analysis includes assessments of system reliability, energy conversion efficiency, and hydrogen output across different seasons.The results highlight the potential of this hybrid approach to provide clean and renewable energy solutions for hydrogen production, thus reducing dependence on fossil fuels and addressing global energy challenges. This work underscores the importance of integrating renewable energy systems in remote areas to support sustainable development and energy transition strategies.

Keywords: *Green hydrogen, hybrid PV-wind system, DC-DC conversion, off-grid solutions, electrolysis.*

Abstract:

Cette étude examine la faisabilité de la production d'hydrogène vert dans le désert algérien à travers un système hybride hors réseau combinant l'énergie solaire photovoltaïque et l'énergie éolienne, intégré à un processus d'électrolyse. L'abondance des ressources solaires et éoliennes dans la région en fait un site idéal pour la production d'énergie durable. Le système proposé repose sur une technologie avancée de conversion DC-DC, visant à optimiser le transfert d'énergie des sources renouvelables vers l'électrolyseur, garantissant ainsi une production efficace d'hydrogène même dans des conditions environnementales variables. L'analyse de performance inclut l'évaluation de la fiabilité du système, de l'efficacité de conversion énergétique, et de la quantité d'hydrogène produite à travers les différentes saisons. Les résultats démontrent le potentiel de cette approche hybride pour fournir des solutions énergétiques propres et renouvelables pour la production d'hydrogène, réduisant ainsi la dépendance aux combustibles fossiles et répondant aux défis énergétiques mondiaux. Ce travail met en lumière l'importance de l'intégration des énergies renouvelables dans les zones isolées pour soutenir le développement durable et les stratégies de transition énergétique.

Mots-clés *: Hydrogène vert, système hybride photovoltaïque-éolien, conversion DC-DC, solutions hors réseau, électrolyse.*